technische universität
dortmund

2013

SCIENTIFIC HIGHLIGHTS

Annual Report

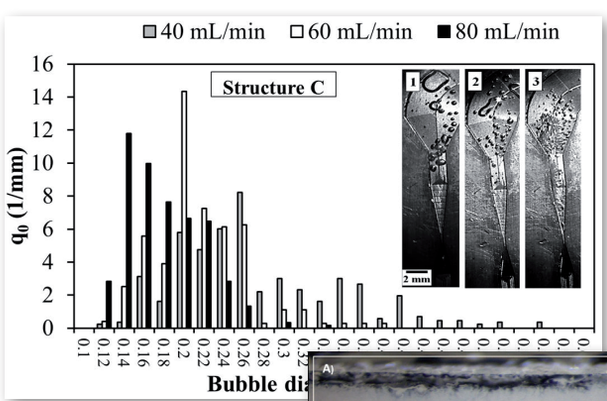

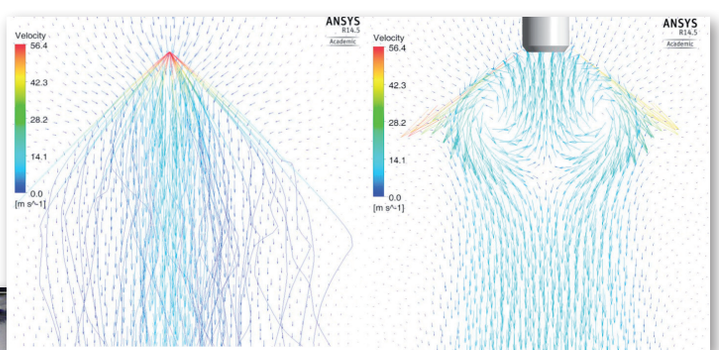

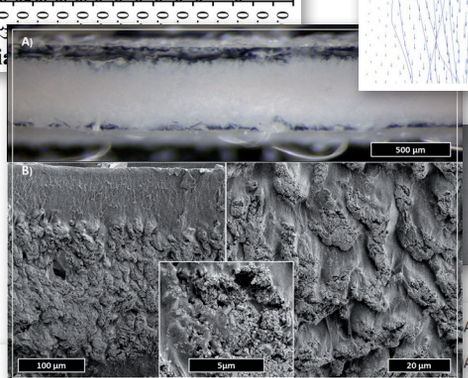

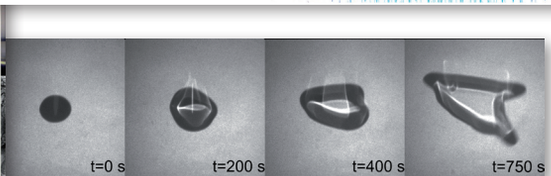

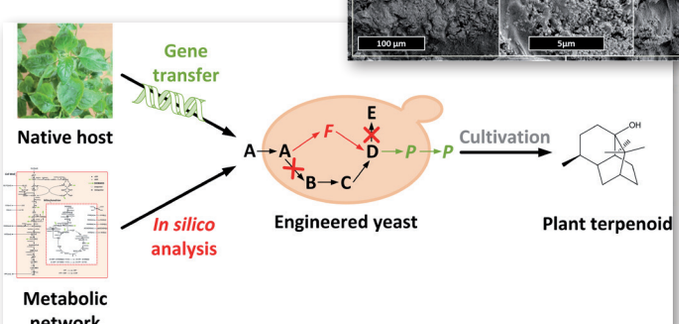

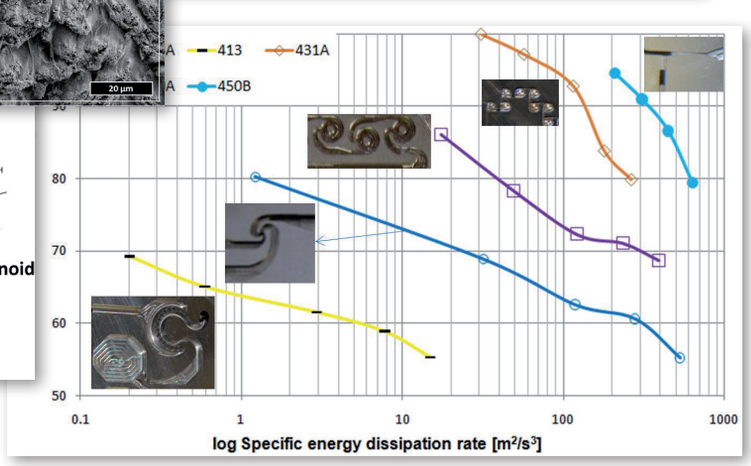

Fakultät Bio- und
Chemieingenieurwesen

Content

Department of BCI 4
Preface 5

Equipment Design (AD) 6
Dispersion in modular channel systems 7
Extraction in millistructured stirred-pulsed columns 8
Liquid-Liquid Mass Transfer in Microchannels 9

Plant and Process Design (APT) 10
Knowledge aided downstream process synthesis 11
Characterization of crystalline products by determining agglomeration degree distribution using image analysis 12

Biomaterials and Polymer Science (BMP) 14
Amazing Rubber 15
Antimicrobial bioswitchable Poly(2-oxazoline)s 16
Semipermanent antimicrobial coatings 17
Smart Polyethylene 18
Enzyme-induced production of shell-like composite materials 19

Chemical Biotechnology (BT) 20
High-resolution growth analysis of isolated single cells 21
D-Xylose assimilation via the Weimberg pathway by solvent 22
Biocatalytic hydroxylation in flow 23

Biochemical Engineering (BVT) 24
Immobilized mushroom cells for removal of bisphenol A 25
Fermentative production of di-rhamnolipids with integrated product capture 26

Chemical Reaction Engineering (CVT) 28
Non-catalytic methane pyrolysis 29
Parallelisation of liquid-liquid-slug flow in microchannels 30
Post-Combustion Carbon Dioxide Capture 31

Process Dynamics and Operations (DYN) 32
Multi-stage Nonlinear Model Predictive Control 33
Guaranteed parameter estimation of dynamic systems 34
Data-driven Adaptive Robust Control 35

Content

Fluid Separations (FVT) 36
Chemo-Enzymatic Reactive Distillation 37
Hyperbranched polymers as phase forming components in aqueous two-phase extraction 38

Particle Technology (MV) 40
Electrostatic precipitators 41
Fast determination of protease activity on gelatin substrate 42
Pattern of conical gas jets and sprays 43

Fluid Mechanics (SM) 44
Spreading of liquid droplets 45

Technical Biochemistry (TB) 46
In silico profiling of *Escherichia coli* and *Saccharomyces cerevisiae* as terpenoid factories 47
Endophytes as antivirulence agents 48

Technical Chemistry (TC) 50
Catalysis with Pd-nanoparticles 51
Epoxidation of methyl oleate in an aqueous biphasic medium 52
Hydroamination of β-myrcene and catalyst recycling by TMS 53
First rhodium catalyzed hydroformylation of cyclopentadiene 54
Self metathesis of fatty acid methyl esters 55
Rhodium-catalyzed codimerization of n-butenes with allylic halides 56
Characterizing Electrochemical Oxygen Reduction Reaction (ORR) 57
Highly selective dimerization and trimerization of isobutene 58

Thermodynamics (TH) 60
Salt Influence on Thermodynamics of Biological Solutions 61
Thermodynamic modelling of protein solubility 62
Thermodynamics of pharmaceutical cocrystals 63
Solubility enhancement of amorphous versus crystalline pharmaceuticals 64
Phase behavior of solid dispersions 65
Modeling Aqueous Two-Phase Systems 66

Department of BCI

Preface

Dear Reader,

I am proud to present the Scientific Highlights 2013 of the Faculty of Bio- and Biochemical Engineering to you. As in the previous three volumes, the BCI is briefly describing the Best of Research of the past year organized by the respective research groups. All abstracts are written for students in Dortmund and other universities, for our fellow researchers and interested colleagues in the industry. The great diversity in the highly interdisciplinary mostly applied research is one of the markings of the BCI faculty, which consists of a productive mixture of engineers and natural scientists.

Besides numerous publications in established, international scientific journals, the application oriented research has led to a number of patent applications and implemented industrial processes in chemical as well as biochemical engineering. Due to the structure of the teaching, students are involved in this successful research in their bachelor, their master as well as their PhD studies. The mixture of scientific background and application-driven research is one of the reasons for the great success of our absolvents in job applications in the chemical and biochemical as well as the pharmaceutical industry.

We hope that this brochure attracts the interest of students to join our research groups and academic as well as industrial researchers to find collaboration partners here.

Enjoy the reading,

Joerg Tiller

Equipment Design (AD)

Dispersion in modular channel systems

Intensified process for mass transfer limitations

Alexander Tollkötter, Norbert Kockmann

The application of microchannels is often limited to the laboratory scale or the production of fine chemicals due to large pressure losses for high flow rates. The flow of microbubbles in millichannels offers reduced pressure loss with simultaneous large specific contact surface. Bubble coalescence in the channels has a contrary effect, which is minimized by continuous re-dispersion in micro nozzles. The transformation of pressure into kinetic energy creates an aimed secondary flow leading to bubble break-up. A modular re-dispersion system with different nozzle and channel modules was studied experimentally and by CFD simulations. All modules are arranged in a plate holder and fixed under a glass plate for optical characterization. Bubble diameters and size distributions show a linear relation of smaller bubbles with larger energy input.

The novel modular microreactor for generating a continuous fine dispersion by flow through Venturi nozzles consists of a block for temperature control, a reaction plate and a view glass fixed by two external flanges, see Fig 1. The view glass is pressed on the reactor plate for sealing purpose and optical characterization. A notch was milled into the reaction plate to place five modules in it: an inlet and outlet module together with three channel modules. Different designs of the nozzles were fabricated with hydraulic diameters from 0.1 to 0.5 mm. Lateral holes were drilled into the plate for fluid and sensor connections. Standard 6 mm pipe fittings were installed to connect the reactor to peripheral equipment.

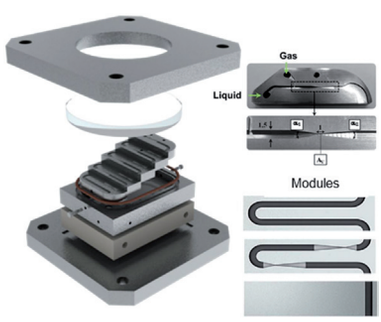

Figure 1: Concept of the modular microreactor with different modules and significant dimensions of an inlet module.

Nozzle geometry was investigated regarding its function of generating fine bubbles. Volume flow rates were investigated from 20 to 500 mL min^{-1} with different phase ratios and observed by a high-speed camera. Pressure loss increased up to 5 bar depending of the nozzle dimensions. Compared to conventional microchannels, this value is much lower for similar flow rates. Inlet and outlet angle of the nozzle should be smaller than 8° for the investigated volume flow rates to avoid additional pressure losses and flow detachment. Bubble size distributions were determined for each nozzle and volume flow rate with diameters from 0.1 to 0.7 mm, see Fig. 2. Higher flow rates resulted in larger pressure drop and energy dissipation. This generally leads to smaller bubble diameters and narrow size distributions. A linear relation between energy input and bubble diameter was identified.

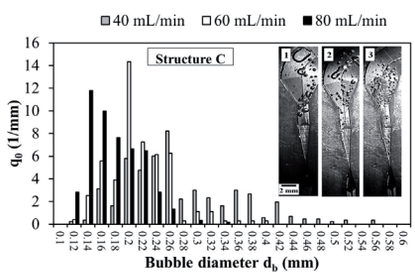

Figure 2: Bubble size distributions of the gas/liquid flow through structure "C" (0.25x0.25 mm2) for flow rates from 40 to 80 mL min-1.

Future work will focus on design of improved channel structures to mitigate bubble coalescence in detachment zones. Furthermore, characteristics of reactive systems will be studied together with residence time distribution, see Fig. 3.

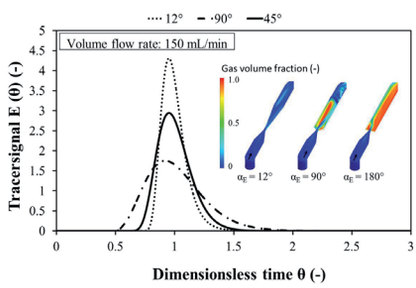

Figure 3: Residence time distributions calculated by CFD simulations for different outlet angles using ANSYS CFX v13.

Contact:
alexander.tollkoetter@bci-tu-dortmund.de
kockmann@bci-tu-dortmund.de

Publications:
A. Tollkötter, L. Lotte, N. Kockmann, Redispergierung von Gas/flüssig-Strömungen im modular aufgebauten mikrostrukturierten Reaktor, Chemie-Ingenieur-Technik, 85, 1430, 2013.
A. Tollkötter, N. Kockmann, Investigation on the bubble detachment from a submerged micronozzle in microchannel flow, poster contribution, ECCE Annual Meeting, The Hague, 22. - 24.4.2013.

Extraction in millistructured stirred-pulsed columns

Intensified process for complex separations

Alexander Holbach, Norbert Kockmann

The downstream process and purification of biochemical and pharmaceutical products represent a big part of the production cost. Process intensification is one important task to make the industry more economically and ecologically sustainable. The intensification is possible on several levels. The first level is the inter- and intramolecular level with the spatial and thermodynamic background. The second level describes the equipment with intensification of the mass transfer and the third level the intensification of the whole process with use of specific interactions of unit operations and exploitation of synergy effects. The objective of this work is to control the fluid dynamics on the millimeter and sub-millimeter scale inside the equipment and to use the positive effects of enhanced heat and mass transfer.

We investigated the process intensification in millistructured extraction columns, with an inner diameter of 15 mm, see figure 1. The column has 50 stirred cells and an active extraction height of 1.1m. With stirred cells we achieved high energy input, high specific surface, and, thus, good mass transfer.

The hydrodynamics and mass transfer inside the column was characterized with the European Federated Chemical Engineering (EFCE) test system n-butylacetate(d)/acetone/water(c). Hereby 25 theoretical stages per meter are realized [1,2]. This is more than twice as already achieved in other miniplant columns. The experiments show that the combination of stirring and pulsation allows for high extraction efficiency for small scale applications.

As an example the enantioselective extraction of (R/S)-α-cyclohexyl-mandelic (CHMA) acid was investigated. The enantioselective extraction is an organic/aqueous reactive extraction. The enantiomers create in the aqueous phase a complex with hydroxy-propyl-ß-cyclodetrin (HP-ß-CD), see figure 2. The (S)-complex is preferred to the (R)-complex, so that the extraction is selective.

The whole process is mass transport limited and has a low selectivity. In conventional columns the extraction is impossible, because the retention time of the dispersed phase and the specific surface between the two fluids are too small. In process intensified extraction columns with high specific surfaces and many extraction stages the counter current extraction shows a good purification for the (R)-enantiomer. First results show a separation of the two enantiomers up to an enantiomer excess of 55 % [CIT].

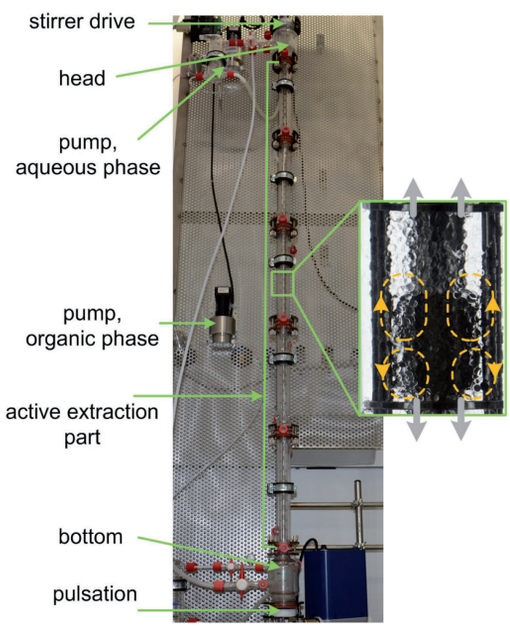

Figure 1: Process intensified extraction column.

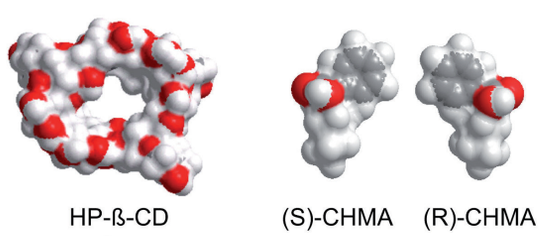

Figure 2: Selector molecule hydroxy-propyl-ß-cyclodetrin (HP-ß-CD) and guest molecules (R/S)-α-cyclohexyl-mandelic (CHMA).

Publications:
[1] A. Holbach, E. Çalışkan, D. Jaritsch, N. Kockmann, Prozessintensivierung mit millistrukturierten Extraktionskolonnen für Stofftransport-limitierte und reaktive Systeme, Chemie-Ingenieur-Technik, 85, 1385-1386, 2013.
[2] A. Holbach, N. Kockmann, Process Intensification in Millistructured Extraction Columns, AIChE Annual Meeting, San Francisco, October 31 to November 8, 2013.
[3] A. Holbach, N. Kockmann, Microchannel Device for Droplet Generation, Mixing, and Phase Separation for Counter-current Flow Extraction, ASME-ICNMM2013-73106, Sapporo, Japan, June 17-19, 2013.
[4] A. Holbach, N. Kockmann, Microstructured stirred-pulsating extraction column, poster contribution, ECCE Annual Meeting, The Hague, 22.-24.4.2013.

Contact:
alexander.holbach@bci-tu-dortmund.de
kockmann@bci.tu-dortmund.de

Liquid-Liquid Mass Transfer in Microchannels

Compact equipment for intensified processes

Alexander Holbach, Norbert Kockmann

Multiphase flow is often found in chemical engineering, food processing, or analytics. First contacting and droplet generation as well as coalescence and re-dispersion have high importance for the flow characteristics. The hydrolysis of ethyl acetate as organic phase with sodium hydroxide NaOH in the aqueous phase is investigated as flexible test reaction for mass transfer characteristics. The consumption of NaOH is used for calculation of specific area and related mass transfer coefficient.

Microchannel setup is also used for liquid-liquid extraction purposes with the aim of counter-current flow arrangement. A device with three microstructured glass plates, droplet generators and phase seperators was developed and experimentally tested to perform a three-step counter-current flow extraction.

A chemical reaction system is utilized to characterize mass transfer and interfacial area in liquid-liquid flow with tunable characteristic times from few seconds to ten and more minutes. Correlations from literature are compared and serve as basis for interpretation of experimental data. The hydrolysis of ethyl acetate enables characterizing mass transfer in reactors with residence time from few seconds to several minutes. The consumption of NaOH in the reactor and adjacent tube is used for calculation of the specific area and related mass transfer coefficient. Different channel geometries are characterized and design considerations are conducted, see Fig. 1. First contacting element has high relevance for the mixing and dispersion process. Typical residence time is important for the suitability of the chemical system.

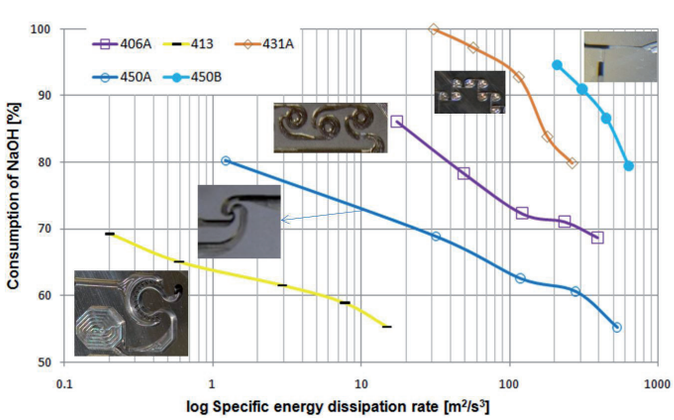

Figure 1: NaOH consumption over energy dissipation rate in the reactor plate.

Microfluidic droplet flow was investigated in a liquid-liquid contacting unit with micro- and millichannels in counter-current arrangement. A contacting module consists of a droplet generator, a channel to enable an intensified mass transfer between the two fluids and a liquid-liquid separation device. Experiments were carried out with deionized water as continuous phase and n-nonane as dispersed phase. The organic droplets are generated by direct coflowing injection through a needle located in the center of the microchannel. The mass transport was studied by a fast acid-base neutralization reaction. The separation unit at channel outlet continuously operates for monodisperse droplet flow. Combined effects of gravity, wetting characteristics of the wall material, and capillary forces nearly completely separate the two fluids over a wide range of flow rates. Based on the mixer-settler system, a microfluidic extraction unit is proposed, which enables a multistage counter-current arrangement, see Fig. 2.

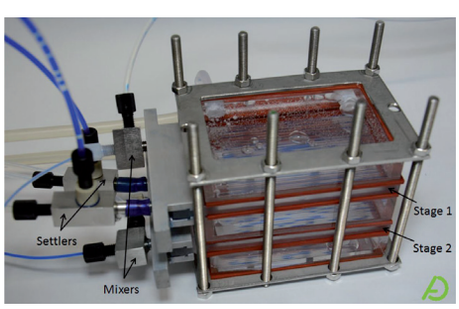

Figure 2: Counter-current arrangement in a glass plate stack with droplet generation + separation (channel size: Ø = 1 mm; L = 2 m; V = 3.8 mL).

Our work shows the possibility of microfluidic droplet operations in micro and millichannels for chemical reactions and liquid-liquid extraction. The general setup with droplet generation, channel flow and separation allows for good and modular application for co-current and counter-current liquid-liquid processes. The counter-current arrangement needs additional pumps for the dispersed phase to flow against the pressure profile. However, there are still major challenges for the counter-current arrangement of droplet flow contactors.

Contact:
alexander.holbach@bci-tu-dortmund.de
kockmann@bci.tu-dortmund.de

Publications:
[1] A. Holbach, E. Çalışkan, D. Jaritsch, N. Kockmann, Prozessintensivierung mit millistrukturierten Extraktionskolonnen für Stofftransport-limitierte und reaktive Systeme, Chemie-Ingenieur-Technik, 85, 1385-1386, 2013.
[2] A. Holbach, N. Kockmann, Process Intensification in Millistructured Extraction Columns, AIChE Annual Meeting, San Francisco, October 31 to November 8, 2013.

Plant and Process Design (APT)

Knowledge aided downstream process synthesis

D. Arndt, K. Backhaus, G. Schembecker

An efficient and innovative downstream process synthesis is the result of many decisions between alternatives of purification processes. Biotechnological products altered the requirements on the downstream throughout the last years. The application of technologies of knowledge based systems and the semantic web, to facilitate the decisions in the future are the subject of this research.

With the cost of the downstream process accounting for up to 50-80% of the overall production costs, young engineers feel the financial pressure on their decisions. Experienced engineers collected enough strategies in their field of work throughout their work life to securely find commercially competitive solutions. Young engineers lacking this hands-on experience have to gain their knowledge through an expert's advice. But especially small and medium businesses do not have own experts in every field. The traditional ways to find a solution are books, scientific papers, or even trail- and error. In this case a lot of alternatives get dropped at an early stage without a proper review of their benefits.

The generation of process alternatives to help young engineers to gain a broader view at their on-hand downstream problem is faced by the implementation of a knowledge based system. Recent developments in the field of the semantic web brought up new technologies to store knowledge in a very extendable way. The use of the Web Ontology Language (OWL) allows representing semantic knowledge in a given domain.

A special challenge for knowledge based systems in the domain of downstream synthesis for biotechnological products is the incompleteness of information. The fermentation broth contains the product and a lot of substances, which are to a certain degree known to the engineer only. One constraint of a highly formal language like OWL is that the description of substances is very strict. A model has been developed in which the engineer is able to provide the information about the substances either as precise number or as a range of five stages.

A methodology has been developed to transform heuristic knowledge from many sources into the formal OWL language constructs. The key aspect in the methodology is to generate positive statements in the processes semantic description (axioms). Making use of the logical monotony of OWLs description logic background, these statements will remain true independent from new added processes or other axioms. A more structural approach to downstream process synthesis is the subject of research at the laboratory of plant and process design for many years. This resulted in a solid basis of heuristic knowledge in this field and structured guidelines in form of decision trees. The analysis and transformation of context bound decision trees into OWL classes formed a big part of the knowledge retrieval process. The knowledge basis in the current version contains 46 different purification processes.

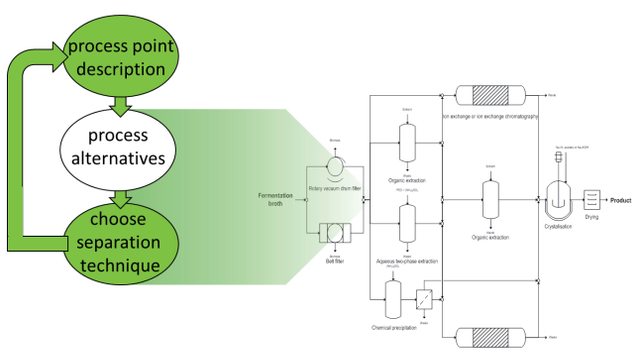

Figure 1: Downstream process synthesis

The application of the ontology is supported by state of the art semantic reasoners. As shown in Figure 1 the generation of a purification strategy is an interactive process. The definition of a situation in the downstream process with its substances and parameters is a process point. With its representation in OWL the reasoner is able to prove logically the applicability of purification processes, resulting in different process alternatives. The consistency of the alternative suggestions has been proven using a set of logical test cases as well as in application of the purification process of Penicilin V as a well-documented literature process.

To ease the generation of process points a web service has been developed, which is able to conceal the OWL aspect of the process point generation from the engineer. Through a variety of drop down menus and a database of substances, the engineer is guided through the process.

Contact:
Daniel.Arndt@bci.tu-dortmund.de
Karin.Backhaus@bci.tu-dortmund.de
Gerhard.Schembecker@bci.tu-dortmund.de

Characterization of crystalline products by determining agglomeration degree distribution using image analysis

L. Terdenge, S. Heisel, G. Schembecker, K.Wohlgemuth

In crystallization a high effort for optimization and process control is made to achieve the desired quality of crystalline products. To evaluate the quality the crystal size distribution (CSD) and responses like median crystal size, width of CSD, or the coefficient of variation are used in general. However, no information about the particle morphology or the amount of agglomerates - further named agglomeration degree - is given by these responses. This lack of information can lead to misunderstand the crystallization process, especially if agglomeration takes place during solid-liquid separation or drying and an off-line CSD measurement technique is used. Therefore, the agglomeration degree distribution (AgD) of crystalline product batches is developed to establish a new quality criterion, which delivers in contrast to CSD information about the amount and distribution of agglomerates.

For the optimization of crystallization processes the detection and localization of agglomeration plays an important role. The techniques image analysis and discriminant factorial analysis (DFA), which is a structure testing algorithm, are used to determine the agglomeration degree distribution (AgD). The steps necessary for the determination of the AgD of a crystalline product batch are shown as a flow chart in Fig. 1.

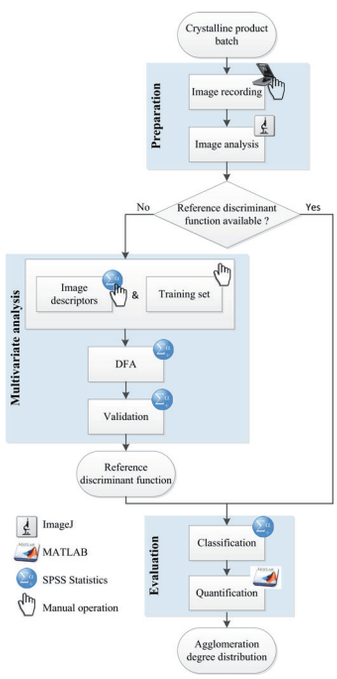

Figure 1: Flow chart for determination of agglomeration degree distribution for a crystalline product batch.

First – during preparation – images of the crystalline particles are taken and each crystal is characterized by several image descriptors using ImageJ. Secondly, in the multivariate analysis step, with the aid of DFA a so-called reference discriminant function is determined. Therefore, approx. 1000 crystalline particles of the product batch have to be first of all classified manually into groups like single crystals and agglomerates to create a training set. Simultaneously suitable image descriptors have to be identified to find a linear combination of image descriptors that separates the elements of the training set with a minimal overlay of the defined groups. To avoid a time consuming manual classification of crystalline particles for each product batch a reference discriminant function is identified during validation, which can be used for all product batches of the same material system. Consequently, the multivariate analysis has to be done only if no reference discriminant function for the material system is available. In the last step – the evaluation – the reference discriminant function is used to classify automatically all crystalline particles and the product batch is quantified by determining the AgD from the agglomeration degree of particle fractions (red crosses) and characteristic values like the maximal agglomeration degree Ag_{max} (see Fig. 2).

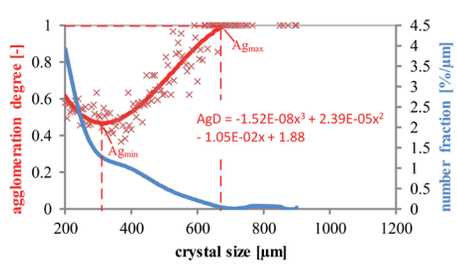

Figure 2: AgD (red) and CSD (blue) of a dried L-alanine/water product batch.

In future research work the AgDs after crystallization and drying should be compared to identify for optimization whether agglomeration takes place during crystallization or further downstream processes.

Publications:
Terdenge, L.; Heisel, S.; Schembecker, G.; Wohlgemuth, K.: Characterization of crystalline products by determining agglomeration degree distribution using image analysis, Jahrestreffen des Fachausschusses Kristallisation (2014), Münster, Oral Presentation.

Terdenge, L.; Heisel, S.; Schembecker, G.; Wohlgemuth, K.: Agglomeration degree distribution as quality criterion to evaluate crystalline products – *in preparation*

Contact:
Lisa-Marie.Terdenge@bci.tu-dortmund.de
Stefan.Heisel@bci.tu-dortmund.de
Kerstin.Wohlgemuth@bci.tu-dortmund.de
Gerhard.Schembecker@bci.tu.-dortmund.de

Biomaterials and Polymer Science (BMP)

Amazing Rubber

Sensing and Memorizing Solvent Vapors

Dominik Quitmann, Nikola Gushterov, Gabriele Sadowski, Frank Katzenberg, Jörg C. Tiller

Natural Rubber (NR) is a renewable, quite old polymer that holds to date an impressive market share with 12 million tons per year which is about a quarter of all rubber materials. Recently, we discovered exceptional shape memory properties for NR whenever it is lightly crosslinked below 0.4%. Now we found a completely new facette of shape memory natural rubber (SMNR). Under certain conditions SMNR is capable of responding to different solvent gas concentrations and simultaneously memorize a formerly applied maximal concentration as well as the chemical nature of the solvent itself.

We found that the contact of programmed SMNR with solvent vapor, e.g. by holding it over an open toluene bottle, causes immediate triggering and complete recovery of its initial state. Unfortunately, any qualitative and quantitative information on the trigger capability of the solvent vapors is lost in this unconstrained experiment. We proposed that fixation of a programmed SMNR will cause a mechanical stress response, that is reversible after removing the solvent.

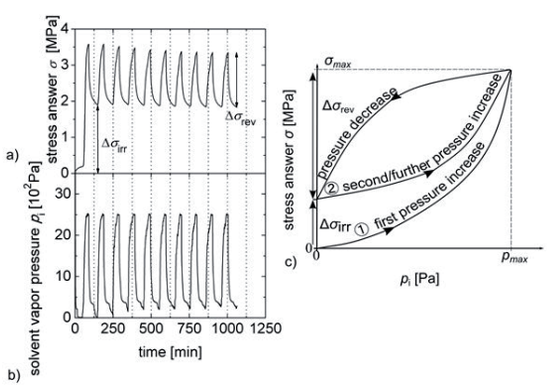

Figure 1: Temporal progress of the stress answer of (composed of a reversible and irreversible part) constrained SMNR with changing solvent vapor pressure.

We found that a programmed SMNR, which is fixed between two clamps, cannot recover its original shape but responds with a tensile-stress when exposed to suited solvent gases, as shown in Figure 1. This stress-answer is composed of a reversible stress $\Delta\sigma_{rev}$ and an irreversible stress $\Delta\sigma_{irr}$ that remains after solvent removal. The reversible stress-answer $\Delta\sigma_{rev}$ is highly sensitive to the applied gas pressure and allows in-situ measurement of the solvent gas pressure p_i for toluene, chloroform, n-heptane, cyclohexane and tetrahydrofuran.

Further, we found that the irreversible stress answer $\Delta\sigma_{irr}$ also carries valuable information since it is only altered when the solvent gas pressure p_i exceeds a formerly applied one. Thus the maximal solvent gas pressure p_i applied to the sample can be read out by measuring the irreversible stress answer $\Delta\sigma_{irr}$.

Furthermore, this solvent concentration dependent irreversible stress answer can be reset by heating the constrained SMNR to a temperature of 80°C.

Thus, the exposure of constrained SMNR to a solvent writes a solvent- and concentration-dependent signature to its microstructure which can be deleted by heating (concept illustrated in Fig. 2).

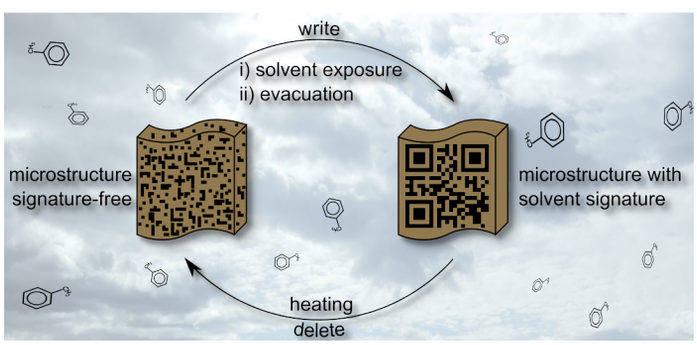

Figure 2: Schematic illustration of the solvent memory effect of shape memory natural rubber (SMNR).

In summary, SMNR is an amazing, highly responsive material that is capable for in situ sensing solvent gas concentrations and, furthermore, memorizing applied maximal solvent gas pressures in the sense of an Erasable Programmable Read Only Memory (EPROM).

Contact:
dominik.quitmann@tu-dortmund.de
frank.katzenberg@tu-dortmund.de
joerg.tiller@tu-dortmund.de

Publications:
D. Quitmann, N. Gushterov, G. Sadowski, F. Katzenberg, J. C. Tiller, Applied Materials & Interfaces 2013, 5, 3504-3507

D. Quitmann, N. Gushterov, G. Sadowski, F. Katzenberg, J. C. Tiller, Advanced Materials 2014, DOI: 10.1002/adma.201305698

Antimicrobial bioswitchable Poly(2-oxazoline)s

How to control the antimicrobial activity of polymeric biocides by altering end groups

Christian Krumm, Simon Harmuth, Montasser Hijazi, and Joerg C. Tiller

Biocides are killing pathogenic germs in our surroundings and protect surfaces from bio-fouling. Unfortunately, the massive use of biocides and antibiotics helps developing of resistant pathogenic bacteria, which are presenting one of the greatest challenges in modern medicine. Further, they are found everywhere and cause unpredictable long-term environmental problems. Thus, a biocide which can be deactivated after its application would be helpful to reduce the spread of microbial resistances. We have designed such a modern biocide based on antimicrobial poly(2-methyloxazoline)s by using a bio-renderable end group, the so-called satellite group (SG).

The antimicrobial activity of polymers with a biocidal group at the end of biologically inert PMOx is greatly controlled by the nature of the group at the other end of the macromolecule. We proposed that this so-called satellite group effect might be used to switch the antimicrobial activity of a whole macromolecule by just changing the satellite group. Figure 1 shows the concept of this approach on the example of a PMOx with an ester SG and the biocidal group N,N-dimethyldodecylamine DDA.

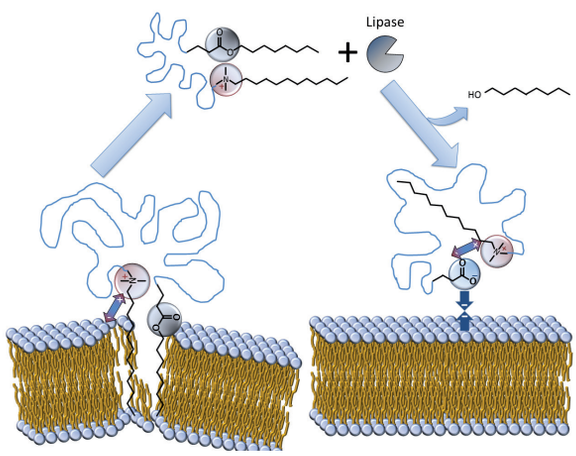

Figure 1: Schematic representation of the membrane-active biocidal DDA-PMOx controlled by the cleavable satellite group before and after hydrolysis.

A series of such polymers was synthesized introducing the ester by the initiators for the cationic ring-opening polymerization of 2-methyl-2-oxazoline and terminating the polymer with DDA. The ester SG was hydrolyzed by treatment with aqueous NaOH. NMR spectroscopy and electron spray ionization mass spectrometry revealed that the ester cleavage is quantitative and no other group of the macromolecule is affected by the procedure, proving selective cleavage.

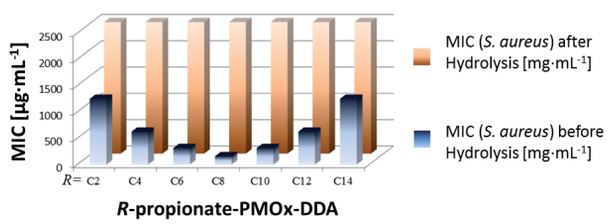

Figure 2: Minimal inhibitory concentrations of the antimicrobial telechelic PMOx before and after hydrolysis of the satellite group.

The polymers were investigated with regard to their antimicrobial activity against the GRAM-positive bacterium *Staphylococcus aureus*. The PMOx with the octyl ester SG revealed the highest antimicrobial activity (156 µg·mL^{-1}). After ester cleavage the antimicrobial activity of the polymers showed that the carboxylic acid SG completely diminishes the antimicrobial activity of the polymers against the microorganism (Fig 2). We prepared an OP-PMOx-DDA with a shorter chain length of 30 repeating units, and it was found that this polymer is more active against S. *aureus* (MIC 40 µg·mL^{-1}) and the hydrolysis of the SG group of the macromolecule resulted in an MIC against S. *aureus* of 1250 µg·mL^{-1} indicating an activity decrease by a factor of 30.

The hydrolysis of the SG was performed additionally with lipase under physiological conditions. After 3 and 7 days of contact with lipase the MIC values were found to be 156 and 312 µg·mL^{-1}, respectively, while the polymer treated with the buffer without lipase remained fully antimicrobial active. This shows that lipase indeed deactivates the antimicrobial activity of the polymer.

Further, the octyl ester SG-PMOx-DDA polymer showed a very low toxicity for pork blood cells (HC_{50} ~ 5000 g/l), which results in a selectivity value of HC_{50}/MIC(*S. aureus*) of more than 100. This shows that the polymer is not only environmentally friendly but also of low toxicity to mammalians.

Publications:
Christian Krumm, Simon Harmuth, Montasser Hijazi, Britta Neugebauer, Anne-Larissa Kampmann, Helma Geltenpoth, Albert Sickmann and Joerg C. Tiller

Antimicrobial Poly(2-methyloxazoline)s with Bioswichable Activity through Satellite Group Modification Angewandte Chemie Int. Ed. 2014, 53, 3830-3834

Contact:
christian.krumm@udo.edu
joerg.tiller@udo.edu

Semipermanent antimicrobial coatings

Solubility Switching of Star-like Poly(styrene)-block-Poly(4-vinyl-N-methylpyridinium)

Felix Siedenbiedel, Thorsten Moll, Joerg C. Tiller

Rendering surfaces antimicrobial for prevention of biofouling and spreading diseases is an important topic in material science and medicine. Although permanent contact-active bacteria-killing coatings are advantageous, they sometimes render other surface properties in undesirable ways. In order to address this, we have developed a contact-active antimicrobial coating that can be applied from an aqueous solution and forms a coating that resists typical environmental conditions, but can be removed and reapplied deliberately.

Goal of the present work was to develop an antimicrobial coating that can be applied from an aqueous solution and resists short washing cycles and bacterial colonization, but can be rinsed off by thorough washing (Figure 1).

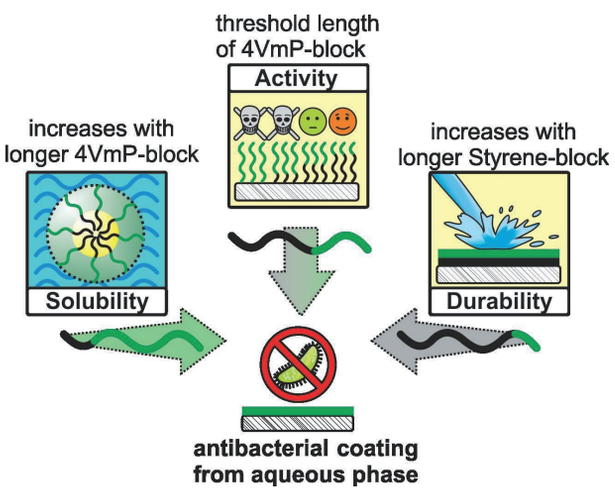

Figure 1: Concept of semipermanent antimicrobial coatings.

To this end a series of star-shaped polystyrene (PS)-block-poly(4-vinyl-N-methylpyridinium iodide) (P4VMP) polymers were synthesized by anionic polymerization using a core-first approach.

The polymer structure in terms of arm-number, -length, and -composition was optimized regarding solubility in water after heating, water-insolubility of a coating formed from this solution and antimicrobial activity. We found that star-polymers with 3-4 arms and P4VMP/PS ratios of 3-7 were best suited regarding the targeted properties. These polymers are insoluble in water, but become soluble after heating to 100°C for 5min (see Figure 2, left).

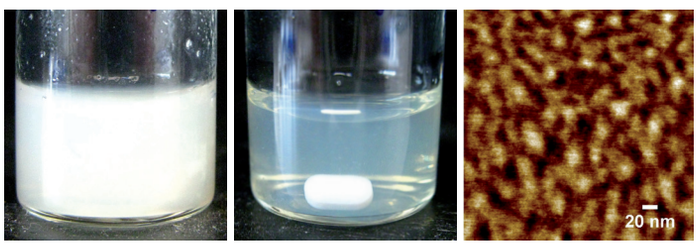

Figure 2: Left: 5 wt% suspension of polymer in water at room temperature and Middle: after heating to 100°C for 5 min Right: AFM image of a cross-section of a coating formed from this solution.

The coatings formed from these aqueous solutions resisted more than 20 flush-like washing cycles. Investigations of these coatings with atomic force microscopy (Figure 2, right) revealed that the change in water-solubility might be due to a transition from unimicellar structures of the star-polymers in solution to network-like structures in the coating.

All coatings were tested regarding their antimicrobial activity against the Gram-positive Staphylococcus aureus and the Gram-negative Escherichia coli. The coatings did kill both bacterial strains with great efficiency.

All coating could be removed by intensive washing with water water, proofing the concept valid.

Contact:
Joerg.Tiller@tu-dortmund.de
Thorsten.Moll@bci.tu-dortmund.de

Publications:
F. Siedenbiedel, A. Fuchs, T. Moll, M. Weide, R. Breves, J.C. Tiller
Star-shaped Poly(styrene)-block-Poly(4-vinyl-N-methylpyridiniumiodide) for semipermanent antimicrobial coatings Macromolecular Bioscience 13 (10), 1447-1455 (2013)

Smart Polyethylene

How to Memorize Multiple Shapes?

Robin Höher, Thomas Raidt, Frank Katzenberg, Jörg C. Tiller

Future superior shape memory polymers (SMPs) will not only react on versatile triggers but also be able to address more than one shape change. So far, multiple shape memory materials are prepared by implementing the multi shape answer in the unchangeable chemical composition. Here we present a new design concept that allows tuning multiple shapes into a material in the programming step. This was approached by manipulation of the microstructure of a polyethylene blend by thermomechanical processing remotely similar to the hardening of metals.

As concept to gain a network with a tunable multi-shape memory we prepared lightly cross-linked blends of three different polyethylenes with overlapping melting regimes in order to get the ability to specifically address each crystal fraction with a separated melting temperature to a respective temporary shape. To this end we chose an HDPE, an LDPE and an EOC with branching contents of 0.5‰, 23‰, and 60‰, respectively. As shown in a previous work each polyethylene exhibits a dual-shape memory with excellent properties, while the trigger temperatures decrease with increasing content of branching. Considering the crystallinity of each PE, we prepared cross-linked blends comprised of 80wt% EOC, 15wt% LDPE, and 5wt% HDPE in order to uniformly distribute the amount of strain stabilizing crystals for each melting temperature. The obtained network can be programmed to a dual- (DSM), triple- (TSM) or quadruple-shape memory (QSM). Depending on the required shape memory up to three intermediate temporary shapes must be correlated to the separately melting crystal fractions of the three PEs. As an example, for a QSM the temporary shape S3 is exclusively stabilized by EOC crystals, while the shapes S2 and S1 are stabilized by LDPE and HDPE crystals, respectively. This is implemented by an elaborate programming procedure comprised of several targeted heating and stretching steps. The obtained retraction versus temperature diagrams of a programmed and fixed DSM, TSM and QSM are shown in Figure 1.

The triple- and quadruple-shape memory exhibit exceptionally well-defined intermediate temporary shapes (retraction < 0.5% K-1) over a significantly broad temperature range (up to 30 K), large storable strains (up to 1700%) and nearly full recovery of all shapes (> 98.9%). Thus, we were able to show a tunable shape memory effect for one and the same material by applying different programming procedures.

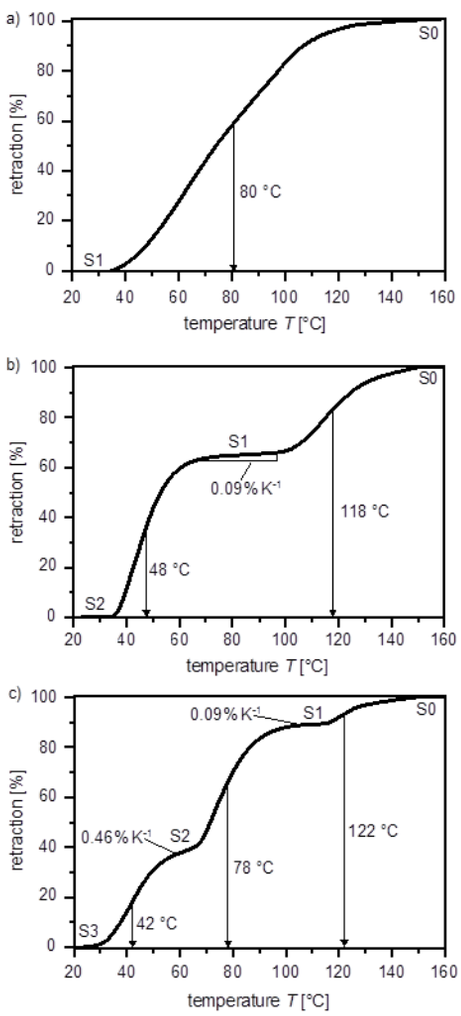

Figure 1: Retraction versus temperature diagram of a cross-linked blend programmed to a) DSM, b) TSM and c) QSM. Arrows indicate average trigger temperatures. S0 = permanent shape, S1-S3 = different temporary shapes.

Publications:
R. Hoeher, T. Raidt, C. Krumm, M. Meuris, F. Katzenberg, J. C. Tiller, Macromol. Chem. Phys. 2013, 214, 2725

Contact:
robin.hoeher@tu-dortmund.de
frank.katzenberg@tu-dortmund.de
joerg.tiller@tu-dortmund.de

Enzyme-induced production of shell-like composite materials

Selective bulk mineralization of a polymer hydrogel resulting in new types of biomimetic composites

Nicolas Rauner, Monika Meuris, Stephan Dech, Julia Godde and Joerg C. Tiller

Numerous approaches were taken to synthetically prepare nature inspired composites like shells, because of their outstanding properties and biocompatibility. Established procedures are quite elaborate and not yet suited to produce materials with dimensions above the microscale. For that reason we developed a new, easy and effective way to produce shell-like $CaCO_3$ composites in large scale based on water-swellable polymers. The therein grown crystals form nanostructured, biomimetic layers, which are capable of improving stiffness of the polymer up to 700-times.

We have developed a novel method of mineralizing bulk materials in larger scale following the approach of enzyme-induced mineralization. The new approach uses immobilized urease to induce and limit $CaCO_3$ crystallization inside a polymer network by an enzymatically catalyzed reaction. As found previously, enzymes can be dissolved in organic mixtures of monomers such as 2-hydroxy ethyl acrylate (HEA) and triethylene glycol dimethacralate (TEG) without losing their activity. This was used to dissolve the enzyme urease in such mixture and photopolymerize those. The formed film contains active urease. These bioactive polymer conetworks were then treated with an aqueous mixture of urea and $CaCl_2$. It was expected that urease hydrolyzes urea to form carbonate within the film, which will precipitate with calcium ions in the bulk followed by crystallization of calcium carbonate. This concept proved valid. The bio-induced calcification indeed allows forming crystals within a short period at room temperature (Figure 1).

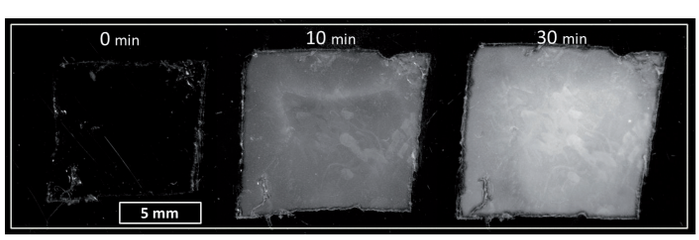

Figure 1: Stereomicroscope images of a hydrogel with entrapped urease treated with an aqueous solution of $CaCl_2$ and urea at room temperature for different periods of time.

The effect of the conetwork composition on the crystal growth was observed. In addition the influence of the degree of polymerization, immobilized urease concentration and temperature of calcification were investigated. All named parameters strongly affect the morphology of grown crystals inside the networks.

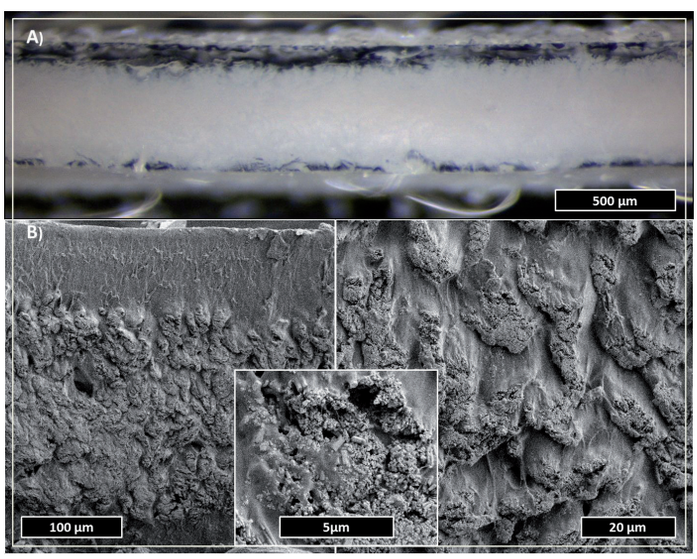

Figure 2: A) Stereomicroscope image of a cross section of PHEA-*l*-TEG conetwork (3 wt% TEG) with entrapped urease (0.5 wt%) treated with an aqueous solution of $CaCl_2$ and urea at room temperature before drying. B) SEM pictures of the same cross section with different magnifications.

That way dense structures of bar-like nanocrystals with different aspect ratios in spherical or dendritic arrays can be formed, which arrange in polymer separated layers (Figure 2). This construction mimics the brick and mortar nanostructures of shell nacre, which results in highly improved mechanical behavior. The grown nanocrystals are capable of increasing stiffness of the starting material up to 700-fold, provided that the microstructure shows a dense construction without pores and strong interaction between crystals and network. The process has the potential to generate a new class of materials that would be available in macroscopic scale for use in light-weight-design and medicine.

Contact:
nicolas.rauner@udo.edu
joerg.tiller@udo.edu

Publications:
N. Rauner, M. Meuris, S. Dech, J. Godde, J.C. Tiller,
Acta Biomaterialia 2014, 10 (9), 3942-3951.

Chemical Biotechnology (BT)

High-resolution growth analysis of isolated single cells

A universal method for quantitative growth analysis at the single cell level

Christian Dusny, Katrin Rosenthal, Oliver Frick, Andreas Schmid

The output of any process involving microbial cells is composed of the physiological activity of each individual cell in the population. Although the average readout of bulk measurements suggests a homogeneous distribution of cellular activity among population members, this is certainly not the case. Studies at single-cell level revealed substantial cell-to-cell differences within clonal populations, occurring on all hierarchical levels from genome to phenome. However, despite extensive research has been performed on the investigation of individual physiology, a universally applicable method for the determination of basal physiological parameters like the specific growth rate has not been established yet.

In this study a universally applicable method for the description of the cell volume at the single-cell level was developed. Using different single-cell analysis systems, growth of single cells was systematically investigated and compared with the corresponding properties of populations. The central assumption behind the determination of the specific volume growth rates based on cell volume increase is a constant density of the cell ρ_{cell} [kg m^{-3}] which is expressed by the ratio of cell mass M_{cell} [kg] to cell volume V_{cell} [m³]ratio.

$$\frac{dV_{cell}}{dt} = \mu \times V_{cell}$$

With this assumption, the specific volume growth rate μ can be described by:

$$P_{cell} = \frac{M_{cell}}{V_{cell}} = const.$$

where V_{cell} is the volume of a single cell or the sum of cell volumes of a population, t is the cultivation time [h] and μ is the specific growth rate [h¹].The actual cell volume was calculated based on a mathematical volume approximation of a segmented club-shaped solid for *C. glutamicum* according to

$$V_{cell} = \frac{2}{3}\pi r_1^3 + \frac{2}{3}\pi r_2^3 + \pi r_1^2 \times (l_1 - r_1) + \pi r_2^2 \times (l_1 - r_1)$$

with r_1 and r_2 [μm] denoting the radii of the spherical poles, and l_1 and l_2 [μm] denoting the lengths of the halves of a cell, respectively.

We cultivated C. glutamicum starting from one cell at standard growth conditions (Fig. 1). In general, growth immediately commenced without any detectable lag-phase upon introduction of the cells into the respective cultivation system.

Measured The increase in individual cell volume was steady and independent of cell size or cellular morphology.

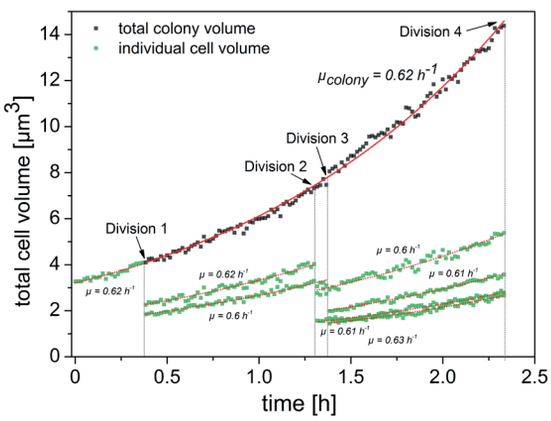

Figure 1: Exemplary determination of specific volume growth rates of single C. *glutamicum* cells during cultivation on agarose pads. The growth experiment started with a single mother cell. Individual cell volume (mother cell and descendants) and total biomass volume of the population were continuously monitored at intervals of 1 min. The mother cell and descending daughter cells exhibited consistent specific volume growth rates that were identical to the specific volume growth rate of the micropopulation.

Descending daughter cells displayed the identical growth rates as the mother cell for at least 3 generations. Consequently, the specific volume growth rate of the individual single cells matched the growth rates of the respective micropopulation.

In conclusion, we developed a universal and straightforward method that allows deriving specific volume growth rates of single cells from any time-lapse microscopy image set. The developed method is comparable to measurements of optical density at the bulk level. We therefore anticipate that growth analysis may be included as a tool for quantitative single cell analysis by default to enable comparison with growth rates obtained at the population level.

Contact:
christian.dusny@bci.tu-dortmund.de
katrin.rosenthal@bci.tu-dortmund.de
oliver.frick@bci.tu-dortmund.de
andreas.schmid@bci.tu-dortmund.de

Publications:
Dusny C., Fritzsch F. S. O., Frick O. and Schmid A., (2012) Applied and Environmental Microbiology 2012, 78, 7132-7136

Rosenthal K., Falke F., Dusny C., Frick O., van den Vlekkert H. and Schmid A., Analytical and Bioanalytical Chemistry 2014, submitted

D-Xylose assimilation via the Weimberg pathway by solvent

tolerant Pseudomonas taiwanensis VLB120

Kirsten A.K. Köhler, Lars M. Blank, Oliver Frick and Andreas Schmid

The natural ability of Pseudomonas taiwanensis VLB120 to use xylose as sole carbon and energy source offers a high potential for sustainable industrial biotechnology. In general, three xylose assimilation routes are reported for bacteria. To elaborate the metabolic capacity of P. taiwanensis VLB120 and to identify potential targets for metabolic engineering, an in silico / in vivo experiment was designed, allowing for discrimination between these pathways. Based on in silico experiments a labeling strategy was developed, ensuring a measurable and unique ^{13}C-labeling distribution in proteinogenic amino acids for every possible distribution between the different xylose metabolization routes. A comparison to in vivo results allows the conclusion that xylose is metabolized by P. taiwanensis VLB120 via the Weimberg pathway.

This study is focused on the description of xylose metabolism in *P. taiwanensis* VLB120, which has not been described before. By means of ^{13}C-isotopomer simulations (Fig. 2) not only different catabolic routes, but also different intracellular flux ratios have been investigated. The complexity of the simulation results underlines the importance of a thorough experimental design as a prerequisite for ^{13}C tracer experiments. It could be shown, that the combined information of five intracellular key metabolites is required for the discrimination between the potential degradation pathways.

The ^{13}C-tracer experiment using 1-$^{13}C_1$-xylose as carbon source showed that only amino acids synthesized from 2-oxoglutarate as precursor are significantly labeled, while amino acids originating from precursor molecules representing the other investigated pathways remained unlabeled (Fig. 2). This means that during xylose metabolization a loss of carbon labeling occurs, that results from the decarboxylation of 2-oxoglutarate to succinyl-CoA, in which the first carbon atom of the substrate is specifically split off and released as $^{13}CO2$.

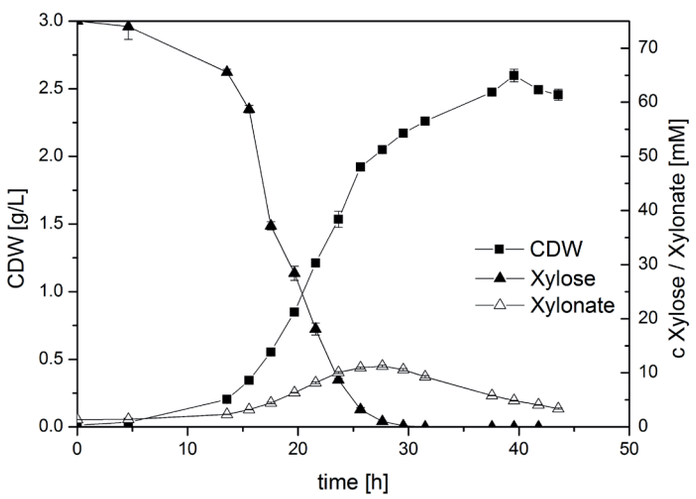

Fig. 1: Growth profile of *P. taiwanensis* VLB120 on D-xylose.

These results strongly point to a xylose catabolism via a catabolic route known as 'Weimberg pathway'. To our knowledge, *P. taiwanensis* VLB120 is the only Pseudomonas strain possessing the Weimberg pathway and so far the only known solvent-tolerant *Pseudomonas* strain, which is able to grow on xylose as sole source of carbon and energy. The direct assimilation via the TCA cycle thereby offers an interesting alternative to the assimilation of glucose via the Entner-Doudoroff and the pentose phosphate pathway. With the background of various previous and significant efforts during the last 20 years aiming for the introduction of an efficient xylose metabolization route into yeast and more recent developments to introduce xylose metabolism into other (solvent-tolerant) *Pseudomonas* strains, *P. taiwanensis* is thus a naturally highly versatile and interesting strain with the ability to convert xylose at high rates. Even without further genetic modification, *P. taiwanensis* VLB120 is well suited for the production of valuable compounds from xylose or mixtures of glucose and xylose, by offering a co-metabolism of xylose and gluconate.

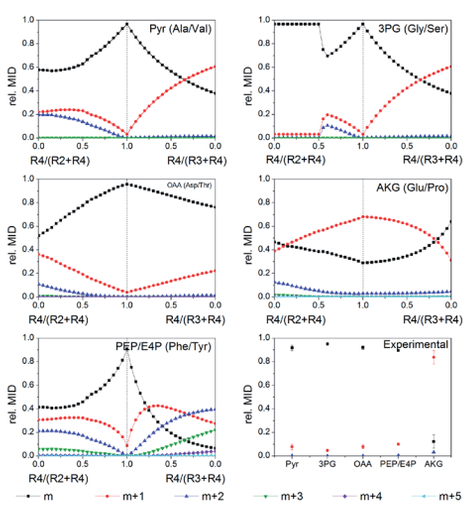

Figure 1: Simulated and experimental labeling distribution of key metabolites for variations of xylose catabolic pathways. $R_4/(R_2+R_4) = 0$: xylose degradation only via PPP. $R_4/(R_2+R_4) = 1$ or $R_4/(R_3+R_4) = 1$: xylose degradation completely via Weimberg pathway. $(R_4/(R_3+R_4) = 0$: xylose catabolism completely via Dahms pathway.

Contact:
Kirsten.Koehler@bci.tu-dortmund.de
Oliver.Frick@bci.tu-dortmund.de

Publications:
K. A. K. Koehler, L. M. Blank, O. Frick and A. Schmid; D-Xylose assimilation via the Weimberg pathway by solvent tolerant Pseudomonas taiwanensis VLB120; submitted

Biocatalytic hydroxylation in flow

Tube-in-tube segmented flow reactor for preparative scale production of catechols

Bartłomiej Tomaszewski, Richard Lloyd, Antony Warr, Katja Buehler, Andreas Schmid

A tube-in-tube microreactor was used for the NADH dependent in-vitro conversion of 2-hydroxybiphenyl to 3-phenylcatechol catalysed by 2-hydroxybiphenyl 3-monooxygenase (HbpA). A biphasic reaction system allowed high substrate loadings whereas the microreactor ensured excellent mass transfer rates between organic and aqueous phases. Oxygen was continuously supplied via membrane aeration over the whole reaction compartment. The productivities achieved were 38 times higher as compared to batch reactions described earlier and almost 4 fold higher than for the same reaction in a micro-reactor in which aqueous, organic and air phases were delivered via consecutive segments. This setup is a promising concept for oxygen dependent biocatalytic reactions in microreactors, and may be regarded as a basis for applications in gram scale organic biosynthesis.

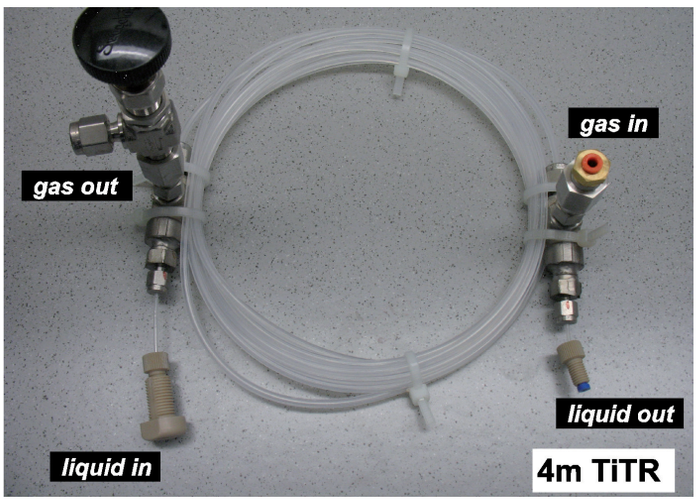

Figure 1: Tube-in-tube reactor (TiTR).

Monooxygenase used in this study is dependent on delivery of oxygen and a hydrophobic substrate, which is hydroxylated. The latter can be delivered in a water-immiscible organic phase thus, in microreactor consecutive segments of aqueous and organic phase are formed. Delivery of oxygen, on the other hand, can be realized either by saturating liquids with air prior to the reaction, or delivering oxygen in an air segment directly into the reactor. Oxygen amount in air segment is however finite and often limits conversions at longer residence times.

To overcome this, a TiTR has been proposed. It consists of a gas permeable Teflon AF2400 membrane tube placed in an outer polymeric tube (Figure 1), thus the respective gas is delivered directly from a pressurized tank via the inner membrane to the liquid phase(s) (Figure 2B). Gas is therefore separated from the liquid reaction components, which simplifies reactor operation, stabilizes the flow and allows for continuous supply of oxygen throughout the length of system (also at increased pressures), keeping its concentration in the reactor at constant level.

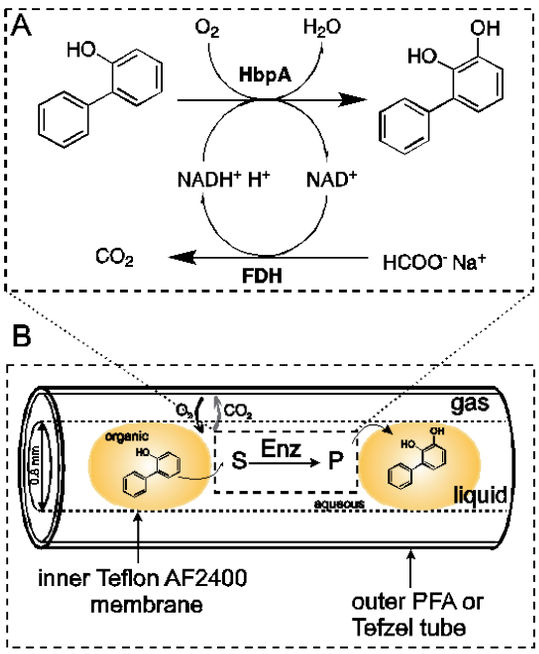

Figure 2: A – Scheme of 2-hydroxybiphenyl 3-monooxygenase (HbpA) catalysed hydroxylation reaction. B – scheme of a TiTR with aqueous/organic two liquid segmented flow.

A successful preparative scale biotransformation in a segmented flow TiTR at 7 bar with continuous oxygen supply has been shown. Product separation was successful and 760 mg of product with excellent purity was isolated. The space time yield of 14.5 g · L_{total}^{-1} h^{-1} is the highest reported for this enzyme. It compares well with an existing industrial process employing oxidoreductases for the synthesis of *tert*-leucine (26.6 g · L_{total}^{-1} h^{-1}).

We anticipate that the TiTR concept will play a significant role for optimizing multiphasic oxygen dependent redox biocatalytic reactions as well as for small scale syntheses for toxicology studies or clinical trials.

Contact:
bartlomiej.tomaszewski@bci.tu-dortmund.de
katja.buehler@bci.tu-dortmund.de
andreas.schmid@bci.tu-dortmund.de

Publications:
Regioselective biocatalytic aromatic hydroxylation in a gas-liquid multiphase tube-in-tube reactor
Tomaszewski, B., Lloyd, R., Warr, A., Buehler, K. and Schmid, A,
ChemCatChem 2014, submitted

Biochemical Engineering (BVT)

Immobilized mushroom cells for removal of bisphenol A

Great potential as a low cost biocatalyst system

Markus Kampmann, Rolf Wichmann

Bisphenol A (BPA) is an important bulk chemical for fabrication of many household plastic products. Due to its endocrine disrupting activity, BPA has received considerable attention, since it has been found in several water streams. The enzymatic oxidation of BPA with tyrosinase has been suggested as a method for the degradation of this anthropogenic contaminant. In order to reduce the cost of enzyme, we have developed a simple and efficient procedure for preparation and immobilization of tyrosinase containing cells from the fruiting body of the edible mushroom Agaricus bisporus. We have demonstrated the capacity of the immobilized cells for degradation of BPA in environmental water samples and could achieve the longest yet reported activity of immobilized tyrosinase in this reaction system.

Pure tyrosinase is expensive to produce on the scales required to be used for catalytic BPA degradation in waste water streams, therefore, cost reduction plays an important role with respect to an industrial application. Tyrosinase is present in the fruiting body of the edible mushroom *Agaricus bisporus*, which is produced in large amounts for human consumption, inexpensive, and readily available throughout the year. Since even simple purification strategies contribute significantly to overall process costs, it is a promising prospect to completely avoid enzyme purification prior to desired application.

Figure 1: A. bisporus before (left) and after immobilization (right)

We have developed a simple and efficient procedure for preparation and immobilization of tyrosinase enzyme utilizing whole cells from *A. bisporus*, without the need for enzyme purification (Figure 1). The cells were entrapped in biopolymer matrix capsules and characterized with respect to their resulting tyrosinase activity. A modification of the matrix material enhanced the activity due to retention of both cells and tyrosinase from fractured cells, which otherwise leached from matrix capsules. The observed activity was similar to the activity that was obtained with immobilized isolated tyrosinase in the same material. Mushroom cells in water were susceptible to rapid inactivation, whereas the immobilized cells maintained 73% of their initial activity after 30 days of storage in water.The immobilized cells were also analyzed for their capacity for the degradation of BPA in repeated batch experiments (24h cycles). Environmental water samples, spiked with BPA, were used as substrate in order to better simulate possible application in an industrial process. BPA conversion was almost 100% for 11 days, under stirring conditions, and 50-60% after 20 days, without stirring (Figure 2).

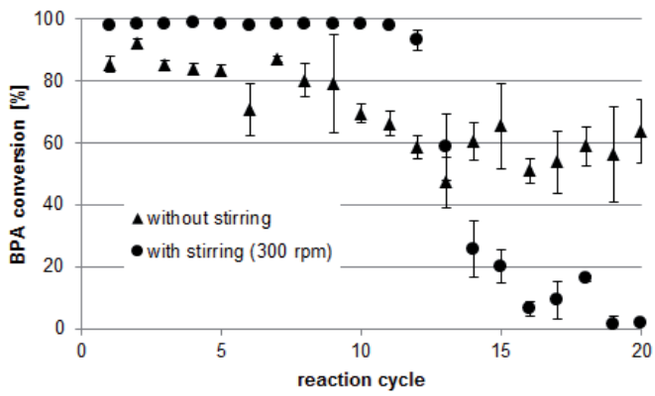

Figure 1: BPA conversions in repeated batch experiments (24 h cycles) with immobilized mushroom cells in environmental water samples, spiked with BPA (0.1 mg/l).

These results represent the longest application of continuous catalytic activity from immobilized tyrosinase based treatment of BPA in environmental water samples reported in literature to date. Therefore, the presented immobilization strategy offers great potentials for reducing the cost of enzyme catalyzed bioremediation processes.

Contact:
markus.kampmann@bci.tu-dortmund.de
rolf.wichmann@bci.tu-dortmund.de

Publications:
Kampmann, M., Kleiner, B., Bielecki, J., Uhl, S., Wichmann, R., Immobilization of tyrosinase in alginate microcapsules for removal of bisphenol A, presentation, 4th Annual CLIB Graduate Cluster Retreat, Lünen, Germany (2013).
Kampmann, M., Kleiner, B., Bielecki, J., Uhl, S., Wichmann, R., Immobilization of tyrosinase in alginate microcapsules for removal of bisphenol A, poster presentation, 9th European Congress of Chemical Engineering and 2nd European Congress of Applied Biotechnology, The Hague, Netherlands (2013).
Kampmann, M., Boll, S., Kossuch, J., Bielecki, J., Uhl, S., Kleiner, B., Wichmann, R., Efficient Immobilization of Mushroom Tyrosinase Utilizing Whole Cells from Agaricus Bisporus and its Application for Degradation of Bisphenol A, Water Research 2014, 57, 295-303

Fermentative production of di-rhamnolipids with integrated product capture

Scaling-up of the production and isolation of rhamnolipids produced by Pseudomonas putida

Benjamin Küpper, Karsten Biss, Christian Nowacki, Rolf Wichmann

Rhamnolipids have a far-reaching potential as an additive in the detergent industry due to surface-active and antimicrobial properties. The goal of this project is the establishment of a successful scale-up of the fermentation process to a scale of about 50 liters of working volume. Furthermore the product has to be captured from the fermentation broth and to be purified in a downstreaming process that has to be adapted to the new vol-umetric scale.

Currently bacterial production strains are developed which enable a very high product yield with relatively little equipment as well as material used. For the last decades, rhamnolipids were produced using the human-pathogenic bacterial strain *Pseudomonas aeruginosa*. However, since this strain belongs to organisms of the safety level 2, it is sought, that genes that are relevant for the production of rhamnolipids are transferred into a related and well-known producer strain (*Pseudomonas putida*) and allow production under S1 conditions on a larger scale.

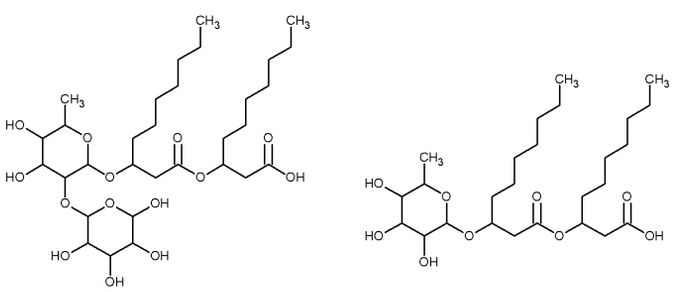

Figure 1: Major Dirhamnolipid molecule (left) and major monorhamnolipid molecule (right).

The scale-up of the fermentative production of monorhamnolipids has been successfully performed from shaker flask scale up to 25 liters of working volume. Due to the larger fermentation volumes, new challenges have occurred regarding the process strategy. One new challenge is to adapt this process to a new molecule in the product spectrum of a *Pseudomonas aeruginosa*. A new production strain (provided by the research group of Professor Lars Blank, RWTH Aachen) is capable of producing di-rhamnolipids as well as mono-rhamnolipids as shown in Figure 1. This new molecule shows a similar behavior regarding foaming and surface active properties. Because of synergetic effects with the other produced rhamnolipids, the performance of a rhamnolipid mixture is even higher compared to a solution that only contains one surfactant. This leads to new and improved application options like in the washing detergent industry or in the field of agricultural industry. The problem of foaming during the fermentation process is now even more present. An elegant way to handle the excessive foaming is a patented procedure, in which the resulting foam leaves directly from the fermenters headspace and is led through a porous bed of adsorbent as shown in Figure 2 (left). Here, the foam collapses due to the adsorption of the surfactants on the adsorbent and leaves the column as a liquid. The higher concentration of the surfactants in the foam enhances this process. With this integrated capture process, a stable fermentation can be provided. The mechanistic build-up still has to be improved for a larger scale. Figure 2 (right) shows a possible set-up for the adsorption column and the flows in detail.

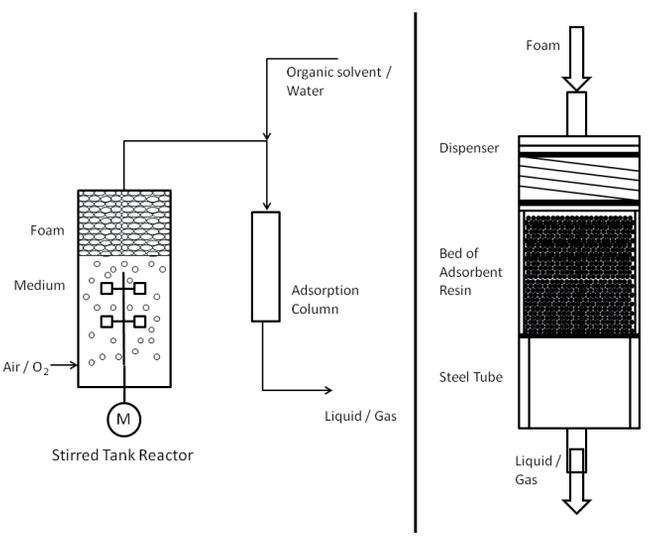

Figure 2: Integrated product separation process (left) and detail of a possible adsorption column attached to a fermenter (right).

Publications:
Oral presentation at Biosurfactant – Challenges and pespectives 2013, Frankfurt/Main „Fermentative Production and Downstreaming of Monorhamnolipids“.
International patent WO2013087674 „Foam adsorption“, 2011

Chemical Reaction Engineering (CVT)

Non-catalytic methane pyrolysis

Generation of hydrogen and energy without carbon dioxide emissions

Dipl. Chem. Ina. Schultz, Prof. D.W. Agar

he use of fossil energy sources is increasingly being dictated by climate change and new means must be explored for using methane as an energy source. Non-catalytic thermal pyrolysis of methane is a promising concept to utilise methane as a hydrogen supply with low to zero carbon dioxide emissions.

Methane can be thermally cracked at temperatures above 600 °C.

$CH_4 \rightarrow C + 2H_2 \quad \Delta H_{1000°C} = +91.7\ kJ$

The use of catalysts and heat transfer surfaces lead to difficulties with carbon fouling.

To achieve high conversions and simplify downstream processing 'lengthy' reaction times (1-10s.) and very high reaction temperatures (>1000°C) are required. Supplying the heat needed convectively via an inert fluid avoids carbon deposition on heat exchange surfaces. Effective heat recovery from the product stream while suppressing the reverse reaction upon cooling makes counter-current flow arrangements separating the carbon and hydrogen formed advantageous.

Use of a ceramic porous-wall reactor, in which heating gas (A_r, N_2, H_2) was supplied radially along the reactor, proved unable to prevent diffusion of methane back into the outer heating chamber despite high flows and back-pressures of the heating medium, which led to rapid and extensive carbon fouling inside and outside the reactor.

A patented gas-liquid slug-flow reactor using molten tin was devised to overcome these difficulties (Figure 1). The molten metal not only serves as a heating medium, but also removes the carbon formed - subsequently separated off as a slag layer - by surface renewal, regulates the reaction time and screens the reactor wall against carbon deposition.

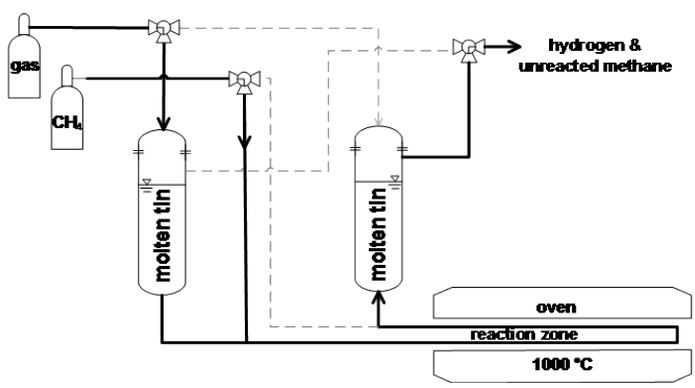

Figure 1: Molten metal capillary reactor

Initial results show that this principle cuts carbon fouling in the reaction zone, even though the molten metal failed to form the anticipated protective film on the quartz glass reactor wall.

Publications:
I. Schultz, D.W. Agar „Decarbonisation of Fossil Energy via Methane Pyrolysis
using two Reactor Concepts: Fluid Wall Flow Reactor and Molten Metal Capillary Reactor", Proc. World Hydrogen Energy Conference, S. Korea 16.06.14 (2014).
D. W. Agar, I. Schultz „Methanpyrolyse im Schmelzmetallkapillarreaktor: Verfahren zur Energie-gewinnung aus Erdgas ohne Erzeugung von umweltschädlichemCO2", Patentanmeldung (2012)

Parallelisation of liquid-liquid-slug flow in microchannels

Non-invasive monitoring and regulation of flow rate and structure

Dipl. Ing. Nicolai Antweiler, Prof. Dr. David W. Agar

Conducting multiphase reactions in micro-reactors is a promising strategy for intensifying chemical and biochemical processes. A major unresolved challenge is to exploit the considerable benefits offered by micro-scale operation for industrial scale throughputs by numbering-up whilst retaining the underlying advantageous flow characteristics of the single channel system in multiple parallel channels. Fabrication and installation tolerances in the individual micro-channels result in different pressure losses and, thus, a fluid maldistribution and even divergent flow structures in different channels.

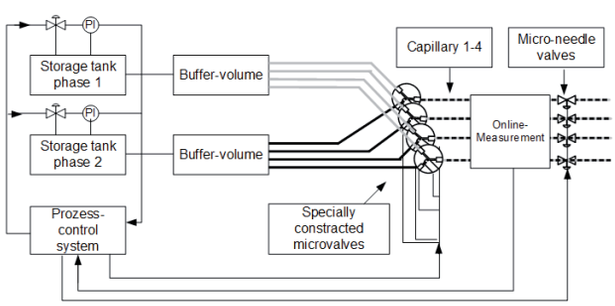

Figure 1: Active control concept for parallel microcapillary reactors

An active control strategy (Figure 1), in which the flow rates and structures monitored in each micro-channel are regulated to harmonise behaviour represents a reliable and flexible solution to this problem, through which the performance of the overall system can be maximised.

A novel non-invasive characterisation of biphasic slug flow has been devised using a single electrode measuring the polarisation arising at the slug phase interfaces, which also yields information on temperature and compositions. Non- invasive techniques for regulating individual liquid flows upstream of the slug mixer by thermal manipulation of viscosity over a restriction element and for controlling slug size via asymmetric voltage application at the mixer have also been developed. CFD-Simulations have been successfully employed to design the alternative microvalves suitable for tuning slug size (Figure 2).

to be improved for a larger scale. Figure 2 (right) shows a possible set-up for the adsorption column and the flows in detail.

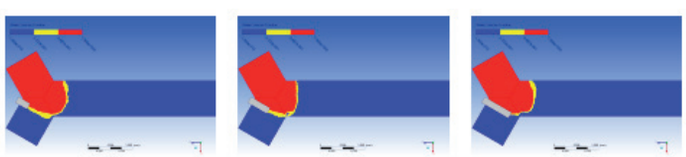

Figure 2: Integrated product separation process (left) and detail of a possible adsorption column attached to a fermenter (right).

These methods permit robust operation of highly parallelised systems at low cost, even in the presence of blockages or the multiplicities, which can be induced by viscosity or slug size changes upon reaction, for example.

Publications:
A.A. Munera-Parra, N. Antweiler, R. Nagpal, D.W. Agar „Stability analysis of reactive multiphase slug flows in microchannels", Processes, 2(2), p. 371-391 (2014).
N. Antweiler, F. Kaske, D.W. Agar " Mess- und Regelkonzepte für die Parallelisierung von Mehrphasenströmungen in Mikrokapillarreaktoren", Chem.Ing.Tech., 84(8), p.1395 (2012).

Post-Combustion Carbon Dioxide Capture

Generation of hydrogen and energy without carbon dioxide emissions

M. Sc. Jiafei Zhang, M. Sc. Yu Qiao, Prof. David W. Agar

Carbon capture and sequestration (CCS) is a crucial stop-gap technology to cut CO_2-emissions from point sources, such as power stations, during the transition to renewable energy sources. CCS-technology presently suffers from several severe technical drawbacks: an extra energy consumption penalty of about 20% and extensive oxidative and thermal degradation of the solvents employed.

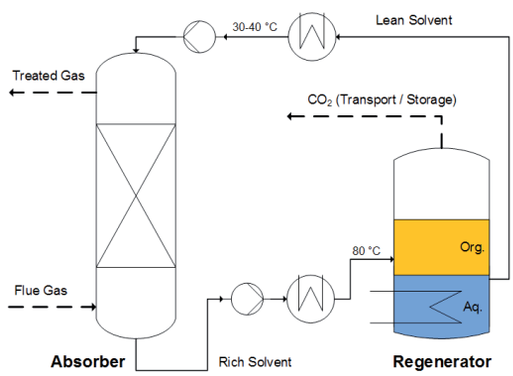

Figure 1: Flowsheet of TBS process

In the laboratory of chemical reaction engineering a patented aqueous blend of amines comprising an absorption activator, a regeneration promoter and a solubiliser has been developed which dramatically reduces both the energy consumption and degradation compared to benchmark processes using alkanolamine (MEA) solutions (Table 1).

The thermorphic miscibility gap induced by raising the temperature of such solvents to ca. 80°C leads to an almost complete auto-extractive CO_2 desorption and, since the solvent can thus be regenerated at lower temperatures than for conventional systems (130°C), one can employ low value, or even waste heat, and drastically diminish the rate of the degradation reactions.

	Sensible heat	Heat of reaction	Stripping	Losses	Total
MEA	0.9	1.8	1.1	0.2	4.0
TBS	0.4	1.35	0.15	0.1	2.0

Table 1: Regeneration energy (GJ/t_{CO2})

The regeneration temperature of 80°C cuts both heat losses and the sensible heat demand of solvent circulation, but the greatest energy saving comes from dispensing with stripping steam. Research showed that intensified agitation, nucleating particles and ultrasonic treatment all gave rise to 'deep' regeneration for very low energy inputs. Potential operational issues, such as packing wetting behaviour, foaming, density and viscosity changes upon loading and volatility losses were found to be either unimportant or remediable through simple countermeasures.

Publications:
J. Zhang, Y. Qiao, W. Wang, R. Misch, K. Hussainy, D.W.Agar „Development of an energy efficient CO_2-capture process using thermomorphic biphasic solvents", Energy Procedia, 37, p. 1254-1261 (2013).
J. Zhang, Y. Qiao, D.W.Agar „Intensification of low temperature thermomorphic biphasic amine solvent regeneration for CO_2 capture", Chem.Engng. Res. Des. , 90(6), p. 743-749 (2012).

Process Dynamics and Operations (DYN)

Multi-stage Nonlinear Model Predictive Control

A new method for model-based optimizing control of nonlinear processes under uncertainty

Sergio Lucia, Sebastian Engell

The presence of uncertainty in real process models prevents the widespread use of model-based optimizing techniques, because the performance and stability of these controllers strongly depend on the accuracy of the models. We present a new method that guarantees satisfaction of the constraints for all possible values of the uncertainties and achieves better performance than other known approaches that are based on a worst-case assumption. Results for an industrial batch polymerization reactor show that the proposed approach leads to significantly shorter batch times than other robust formulations while satisfying the quality and safety constraints for all values of the uncertain parameters.

Model Predictive Control (MPC) is a popular control strategy especially in the process control field mainly because it can deal with constraints on input and states and with nonlinear models (NMPC). MPC uses a model of the system to predict the behavior of the plant and computes a sequence of control inputs that minimizes a certain objective function. The first control input of this sequence is applied to the real system and the procedure is repeated at the next sampling time. For this reason, the performance and stability of MPC controllers relies strongly on the accuracy of the model. Several approaches for robust MPC have been presented in the literature that try to achieve constraint satisfaction and stability for all the possible realizations of the uncertain parameters of the model or of disturbances, at the price of introducing conservativeness in the solution.

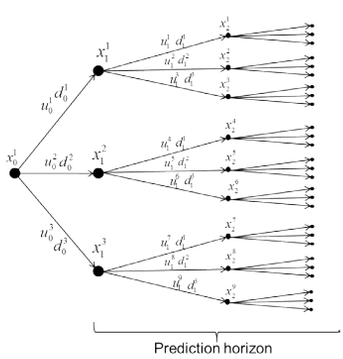

Figure 1: Scenario tree with 3 realizations of the uncertainty

In our work we developed a robust NMPC approach called multi-stage NMPC which takes the uncertainty into account systematically and provides a robust and on the average optimal performance of the plant. The main idea of the approach is to represent the NMPC setting as a real-time decision problem under uncertainty that is formulated as a multi-stage stochastic problem with recourse, based on a description of the uncertainty by a scenario tree (see Figure 1).The representation by scenarios enables the computation of the next inputs taking into account the adaptation of the future inputs to the new information (future measurements) that will be gained at later points in time (i.e recourse). The multi-stage approach has been used for the robust control of an industrial polymerization reactor.

We consider that critical parameters (reaction rate and reaction enthalpy) are uncertain and vary by ±30% around their nominal values. The results of applying standard NMPC and multi-stage NMPC for different values of the uncertain parameters can be seen in Figure 1. Standard NMPC violates the constraints for some realizations while multi-stage NMPC satisfies the constraints for all the values of the uncertainty leading to similar batch times. If other robust approaches are used, considerably longer batch times are obtained.

Future and current work focuses on the rigorous consideration of measurement and estimation noise and on the application to a real reactor.

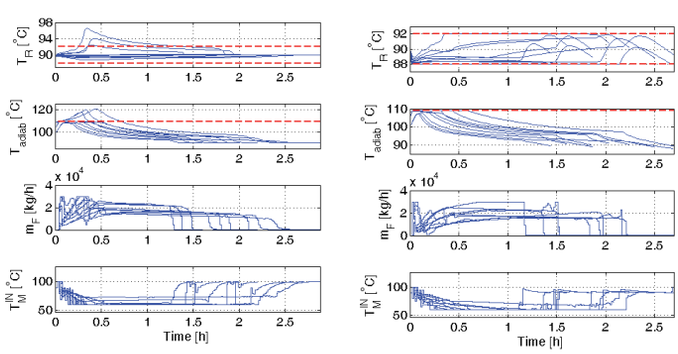

Figure 2: Standard NMPC (left) and Multi-stage NMPC (right) of an industrial polymerization reactor. The plots show the reactor temperature (with constraints), the safety temperature (with constraint), the monomer feed and the jacket temperature. The different lines show different batch runs for different values of the uncertainty.

Contact:
sergio.lucia@bci.tu-dortmund.de
sebastian.engell@bci.tu-dortmund.de

Publications:
S. Lucia, T. Finkler, S. Engell. Journal of Process Control 2013, 23, 1306–1319
S. Lucia, J. Andersson, H. Brandt, A. Bouaswaig, M. Diehl, S. Engell. IFAC World Congress 2014, accepted

Guaranteed parameter estimation of dynamic systems

A rigorous and efficient way to devise confidence limits in parameters of dynamic systems

Radoslav Paulen, Mario Villanueva, Benoît Chachuat

New developments in the domain of finding enclosures to the solutions of parameter-dependent ordinary differential equations together with application of domain reduction techniques open the door to the rigorous and efficient investigation of the quality of information gathered in dynamic experiments for the sake of parameter estimation of dynamic systems such as chemical or biochemical processes. We developed new efficient techniques that enable to guarantee the confidence in the estimated parameters and are ready to be applied to real-world examples.

It is well-known that the state-of-the-art techniques for a posteriori confidence analysis of parameter es-timation of nonlinear dynamic systems yield only approximate and generally imprecise results. In this work, we study *guaranteed parameter estimation* (GPE) of nonlinear dynamic systems. Its goal is to approximate as closely as possible the set of all possible parameter values of dynamic model such that the dynamic quantities, as predicted by the model, match their corresponding measurements within the tolerance of the measurement precision. Thus, GPE provides accurate information on the confidence level of parameters identified from dynamic experiments.

Applied algorithm is based on subsequent partitioning and examination of the space of unknown model parameters. The ability to enclose all the possible solutions of parameter-dependent differential equations is a crucial ingredient for this procedure to be tractable in reasonable computational time. In this respect, we apply newly developed techniques based on *Taylor models*. We also exploit the techniques of domain reduction that enable to enhance the convergence speed of the applied search.

The proof of concept is realized on a rather challenging case study taken from the domain of biochemical engineering. We consider parameter estimation of an anaerobic digester that processes waste water from a winery. The system exhibits complex dynamical behavior occurring on multiple time scales. The two types of biomass are included: acidogenic (A-) and methanogenic (M-) bacteria. The growth rate of A-bacteria is assumed to follow Monod kinetics with kinetic constant K_{S1} and maximal growth rate μ_1. The growth rate of M-bacteria is assumed to follow Haldane kinetics with kinetic constants K_{S2} and K_{I2}, and maximal growth rate μ_2.

The method of guaranteed parameter estimation is applied to estimate the unknown kinetic coefficients of the growth rates. A four-day experiment is considered where the realistic measurement errors are incorporated into simulated data.

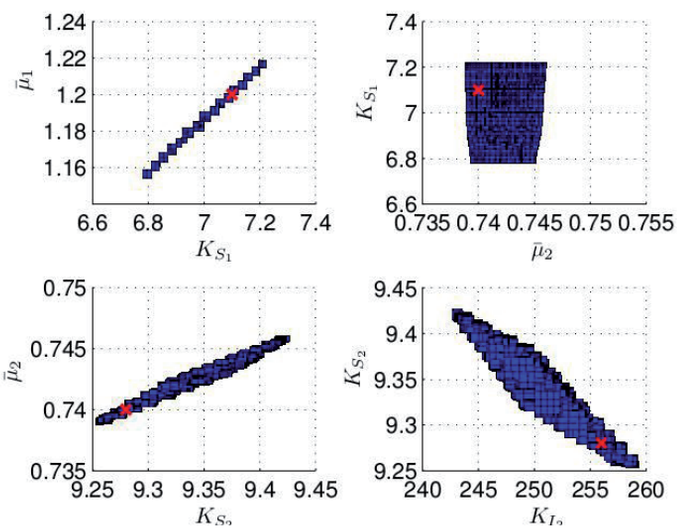

Figure 1: Confidence region of the estimated parameters shown projected to the subspaces (K_{S1}, μ_1), (μ_2, K_{S1}), (K_{S2}, μ_2), and (K_{I2}, μ_2). The red crosses indicate the true parameter values

Moreover, uncertain quantities of the biomass in the digester are considered to be present from the beginning of the experiment. This is done in order to achieve a realistic setup of the problem.

The obtained results are shown in Fig. 1 where the confidence region of estimated parameters is shown projected represent the obtained correlation among the selected pairs of identified parameters. The subsequent analysis showed a significant correlation among the pairs (K_{S1}, μ_1), (K_{S2}, μ_2), and (K_{I2}, μ_2). A minor correlation is observed within the pair (μ_2, K_{S1}). All these observation are expected and are in agreement with the nature of the studied problem and with earlier literature reports. It is notable that similar analysis using the state-of-the-art techniques significantly overestimates the confidence sets reported in Fig. 1.

Our future work concentrates on guaranteed model discrimination and coupling of the proposed technique with online model-based optimizing control for detection of model appropriateness and for its correction.

Publications:
R. Paulen, M. Villanueva, M. Fikar, B. Chachuat, 12th European Control Conf. 2013, 4514–4519
R. Paulen, M. Villanueva, B. Chachuat, IMA J. of Math. Control and Information 2014, submitted

Contact:
radoslav.paulen@bci.tu-dortmund.de
{mario.villanueva10, b.chachuat}@imperial.ac.uk

Data-driven Adaptive Robust Control

Ehsan Gholamzadeh Nabati, Sebastian Engell

The focus of our research is on the development of a model-free adaptive control scheme which is applicable to a wide class of systems and provides a close to optimum performance. To achieve this goal, a data-driven adaptive control approach called unfalsified control is used. This approach requires very little a priori knowledge about the plant dynamics. The original formulation in fact does not match its promises, so we developed and improved version. In particular, our approach includes an optimization of the controller parameters and a criterion to assure robustness.

In various control applications, a classical fixed feedback controller (e.g. PID) does not provide the desired closed-loop performance. Furthermore, in many applications, such as in chemical plants, building dynamic a model of the process is a difficult and expensive task, hence a model-free approach is desirable. One example for such a control application is the control of the steam pressure in an industrial drum boiler. The task is to keep the steam pressure constant by manipulating the fuel flow (Figure 1). In practice the load level of the boiler changes frequently. Thus the controller should be able to deal with large changes in the operating conditions and adapt to them automatically.

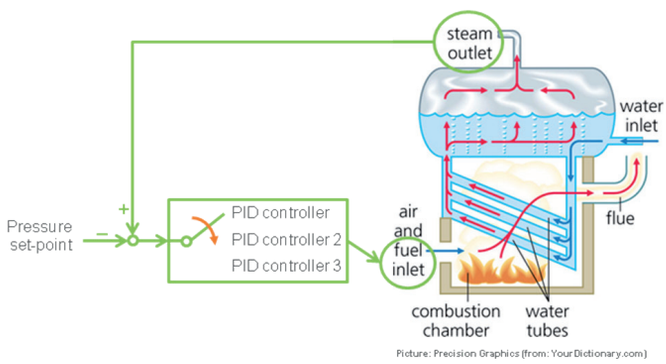

Figure 1: The concept of adaptive control demonstrated on an industrial drum boiler.

To achieve this goal, we use our new adaptive control scheme to control the boiler. In the modified unfalsified control scheme (Figure 2) the adaptive control algorithm switches the active controller, selecting a controller from a set of candidate controllers. The data obtained from the recorded measurements (r, u, y) are used to evaluate the cost of each candidate controller. According to the computed cost values, the best candidate controller is selected by the switching mechanism. In our new approach, the candidate controllers that fail to meet the sufficient condition for robust stability are falsified (i.e. removed from the set). Furthermore, optimization is used to obtain optimal robust candidate controllers if such candidates are not already available in the set.

Contact:
ehsan.gholamzadeh-nabati@bci.tu-dortmund.de
sebastian.engell@bci.tu-dortmund.de

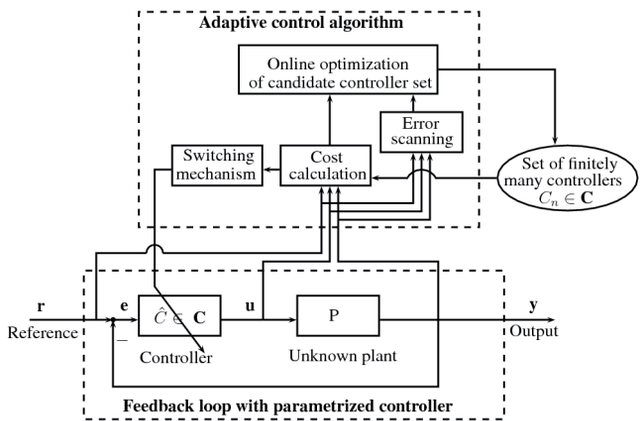

Figure 2: The data-driven adaptive control scheme

(Figure 3) shows how the proposed method improves the performance of the closed-loop by adapting the active controller parameters. Here a comparison is made between the adaptive PI controller and a fixed PI controller. In the simulation the boiler load level changes over time. The variation of load level causes a pressure deviation from its setpoint by 60%. For example a sudden increase of the load level (i.e. steam consumption) leads to a pressure drop hence the controller has to react to this pressure drop by increasing the fuel flow. The results shown in (Figure 3) indicate that the performance of our adaptive controller in reacting to the pressure changes is much better than the performance of the fixed non-adaptive controller.

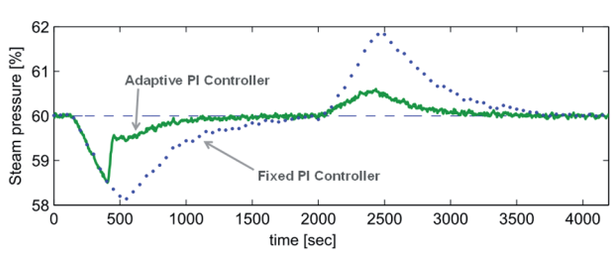

Figure 3: The results of controlling the steam pressure at the boiler outlet.

Publications:
Nabati, E. G.; Engell, S.: Online Adaptive Robust Tuning of PID Parameters, Proc. IFAC Conference on Advances in PID Control (IFAC PID'12), Brescia, Italy, 2012; 625–630
Nabati, E. G.: Data-driven Adaptive Robust Control Based Upon Unfalsified Control. Submitted Dr.-Ing. Dissertation, Dortmund, 2014.

Fluid Separations (FVT)

Chemo-Enzymatic Reactive Distillation

Highly selective and efficient production process for chiral components

Matthias Wierschem, Philip Lutze, Andrzej Górak

Several crucial global challenges such as shortage of material resources in general, energy and water specifically, increasing food demand, environmental pollution and ageing societies as well as the development of new products are drivers for the increasing interest in biocatalytic reactions. Enzymes are enantio- and regioselective, allow for a high selectivity of production processes and are capable of using a wide range of substrates. Enzymes can also be used in bioreactive distillation, which integrates bioreaction and separation in one unit operation to overcome an equilibrium-limited conversion. It creates synergies enabling efficient production of totally new products or existing products using pathways, differing from standard chemical routes.

The chemical production of chiral compounds is still not efficient regarding the energy and raw material efficiency. Separation of these compounds requires substantial investment and energy efforts because of their similar physical properties. Since often only one enantiomer of the chiral compound is applicable, a separation of both is necessary. A bioreactive distillation column for the production of chiral compounds is a promising concept. Bioreaction and separation are integrated in one unit operation to gain synergy effects. The in-situ product removal (ISPR) positively affects the chemical equilibrium of a chemical reaction with a shift to its product site. This is established by either a consecutive reaction or the thermal separation of the components inside a reactive distillation column shown in figure1.

There is a huge variety of possible reaction systems for the chemo-enzymatic reactive distillation which usage is limited by the temperature range of the enzyme and the necessity to use liquid or gaseous substrates or products without solvents. One example of such a reaction system to use in reactive distillation is shown below (figure 1).

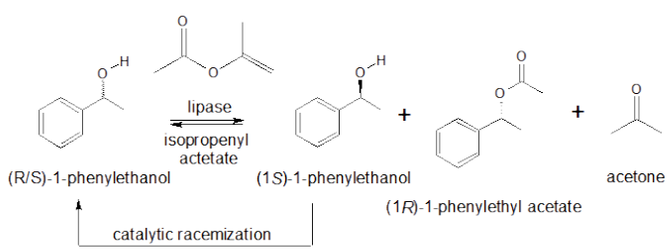

Figure 1: Chemo-enzymatic reaction of 1-phenylethanol

The racemic mixture of 1-phenylethanol reacts with isopropenyl acetate catalyzed by a lipase to form (1R)-phenylethyl acetate. The S form of the supstrate is racemized with a chemical catalyst. The setup of a chemo-enzymatic reactive distillation is shown in figure 2.

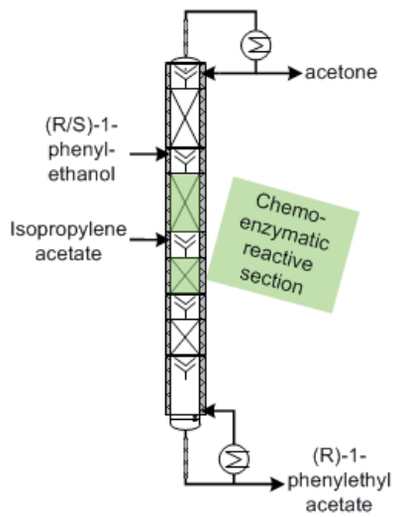

Figure 2: Chemo-enzymatic reactive distillation column

The research objective is the selection of suitable catalysts (chemical and biological), allowing for the column operation at a suitable operating window, the investigation of reaction equilibriums and kinetics, the technical implementation and experimental investigation of the process in a pilot plant column. The vapor-liquid data and reaction kinetics will be determined in order to model the process. To provide the enzyme into the reactive zone, firstly a surface coating and secondly, catalytic packings filled with enzyme granulate can be used. The hydrodynamics of both reactive packings are investigated experimentally to develop suitable correlations for both packings. Then a detailed rate-based model of a reactive distillation is developed and validated against experimental data of a pilot-scale reactive distillation. The validated model is then used to find the optimal operation conditions of the process variables.

Contact:
matthias.wierschem@bci.tu-dortmund.de
philip.lutze@bci.tu-dortmund.de
andrzej.gorak@bci.tu-dortmund.de

Hyperbranched polymers as phase forming components in aqueous two-phase extraction

Investigation and modelling of aqueous two-phase system based on hyperbranched polymer

Andres Kulaguin Chicaroux, Tim Zeiner, Andrzej Górak

Hyperbranched polymers have increased attention in applications because of their special features as branched structure and the wide range of different functional groups. These characteristics make hyperbranched polymers (HB) applicable as phase forming component in aqueous two phase systems (ATPS). They can be used in many bioseparations as alternative to chromatography. As an example ATPS based on hyperbranched polyesteramide and dextran are investigated and compared to an ATPS consisting of polyethylene glycol and dextran. In addition to the experimental investigation of both ATPS, they are modeled using the Lattice Cluster Theory (LCT) in combination with Wertheim theory.

In recent years, the development of pharmaceuticals based on biological based products as monoclonal antibodies has been increased rapidly. Nowadays, chromatography is used as the state of the art technology in the downstream processing of bioproducts. But this technology shows several drawbacks as scale up limitations and ATPS has the potential to overcome these drawbacks.

ATPS can be formed by dissolving two hydrophilic components as two hydrophilic polymers or a salt and a polymer. But the well-known ATPS as the aqueous solutions of phosphate-polyethylene glycol or of dextrane-polyethylene glycol show several disadvantages. On the one hand salts promote the protein aggregation which results in a bad solubility of amphiphilic proteins in the extraction system. On the other hand polymers lead to the high viscosity of coexistent polymer phases.

In order to compensate these disadvantages HB can be used to form an ATPS. Due to the branched structure of HB, this new type of ATPS shows a lower viscosity in both phases compared to linear polymers (figure 1). Moreover, HB are biocompatible and do not cause denaturation of biomolecules.

Essential for the design of an aqueous two-phase extraction is a fundamental knowledge of liquid-liquid equilibrium data and partitioning of target product. However, the experimental investigation of these properties requires enormous experimental effort. To reduce this effort, thermodynamic modeling of ATPS is applied. For the thermodynamic modelling of hyperbranched polymers, the architecture and the influence of functional groups have to be taken into account.

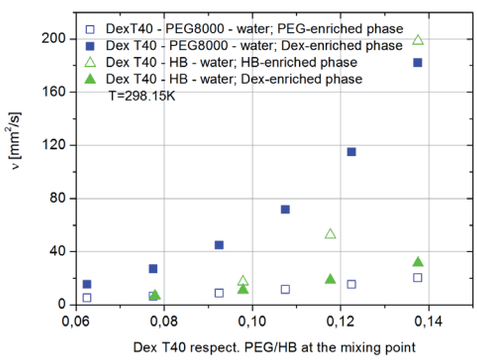

Figure 1: Kinematic viscosity of coexistent phases in ATPS PEG8000-dextran and HB-dextran [1].

Using the LCT, the molecule architecture can directly be considered in the Helmholtz free energy; whereas the influence of polar functional groups is regarded by the Wertheim theory. The results of thermodynamic modeling are shown in figure 2. These results are in sufficient agreement with experimental data. The deviation between experimental data and modelling can be explained by the polydispersity of HB, which is not yet considered in the thermodynamic model. In next step, this model will be extended and tested for quaternary mixtures to predict the partitioning of an amino acid in both studied ATPS.

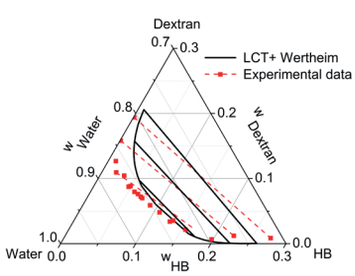

Figure 2: Phase diagram for ATPS based on HB and dextran at 25°C [1].

This work is financially supported by the Deutsche Forschungsgemeinschaft (ZE 990/1-1).

Publications:
[1] A. Kulaguin-Chicaroux and T. Zeiner., Fluid Phase Equilibria, 362, 2014, 1-10.
A. Kulaguin-Chicaroux., T. Zeiner.; Thermodynamische Eigenschaften wässriger Zweiphasen-systeme basierend auf einem hyperverzweigten Polymer, Thermodynamik–Kolloquium 2013, Hamburg, Deutschland

Contact:
andres.kulaguin-chicaroux@bci.tu-dortmund.de
tim.zeiner@bci.tu-dortmund.de
andrzej.gorak@bci.tu-dortmund.de

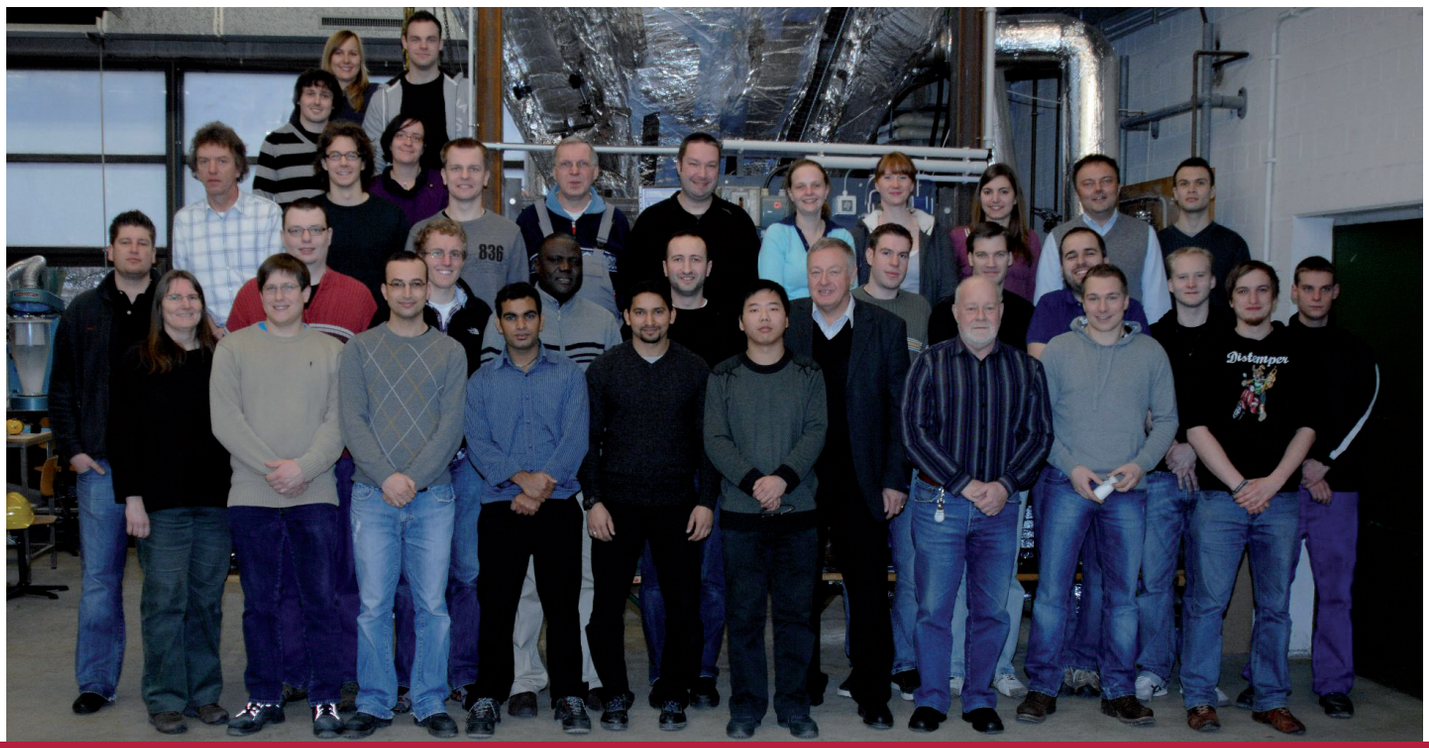

Particle Technology (MV)

Electrostatic precipitators

Measurements of resistivity reveal electret properties of dust

Damian Pieloth, Marcel Rüping, Peter Walzel

The influence of gas temperature and humidity on dust resistivity is well known. The impact of thermic and electric balancing periods on the measurement of dust resistivity is less familiar. The resistivity of particle layers (SiO_2, Al_2O_3 and fly-ash) was measured. The resistivity shows a non-Ohmic behavior regarding the layer thickness and electrical treatment history. Due to this behavior constant values of resistivity were first measured after 16 hours. Sorption curves of H_2O into particle layers show balancing periods of roughly one hour. Hence solely thermal processes cannot explain the balancing periods occurring during the measurement. While thermal and electric balancing periods overlap the latter take a much longer time.

In the study, the influence of thermal and electric balancing periods on the measurement of resistivity was studied. The resistivity balancing periods of SiO_2, Al_2O_3 and fly-ash particle layers were measured as a function of time and particle layer thickness. The measurements were carried out under constant environmental conditions and constant current density through the particle layer (0.5 mA/m²). Typical field strengths required for this current lie in the range of 2 to 10 kV/cm.

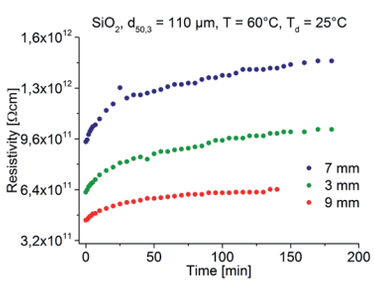

Figure 1: Dust resistivity of SiO_2 particle layers as a function of time and dust layer thickness [1].

Fig. 1 shows dust resistivity of SiO_2 particle layers as a function of time under gas temperature T = 60°C and dew point T_d = 25°C. The resistivity curves cannot be explained by adsorption and desorption of H_2O at and from the particle layers. The total time required for diffusion of water vapor through the particle layers is less than a few minutes as measurements and calculations show. It can be rather assumed that in applying voltage to the particle layer, electric processes are started within the layer which superimpose the mass and heat transfer processes and whose balancing times are much longer than 200 minutes, as Fig. 1 shows.

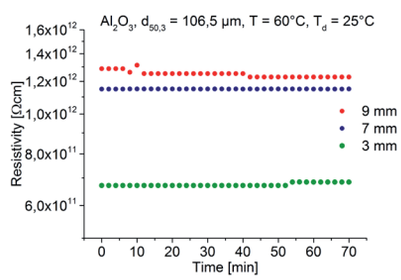

Figure 2: Dust resistivity of Al_2O_3 particle layers after 16 hours thermal and electrical preconditioning [1].

To clarify the balancing periods, measurements with thermal and electrical preconditioning of the particle layer for more than 16 hour at constant gas temperature, e.g. T = 60°C, dew point T_d = 25°C and current density of j = 0.5 mA/m² were carried out. Fig. 2 shows the resistivity of Al_2O_3 particle layers as a function of time with starting the measurement after 16 hours of preconditioning i.e. keeping the sample within the electrical field. With preconditioning the transient behavior of dust resistivity vanishes. In addition it shows increasing resistivity with layer thickness in accordance to the measurements in [2].

The resistivity of particle layers without preconditioning shows non-Ohmic and transient behavior that can be explained by the electret properties of particle layers. In measuring dust resistivity, important for the deposition behavior of dust in electrostatic precipitators the balancing periods and history of treatment should be considered to avoid a misinterpretation of the results.

Contact:
damian.pieloth@bci.tu-dortmund.de
marcel.rueping@bci.tu-dortmund.de
peter.walzel@bci.tu-dortmund.de

Publications:
[1] D. Pieloth, H. Wiggers, P. Walzel, Thermodynamic, material and bulk property influence on electrical resistivity of particle layers, Chem. Eng. Technol. 2014, 37, No. 4, 1-9
[2] U. Riebel, Y. Aleksin, A. Vora, Das elektrische Verhalten hochohmiger Stäube, Chem. Ing. Tech. 2013, 85, No. 3, 235-244

Fast determination of protease activity on gelatin substrate

Visocimetry enables access to degradation of protein chains

Monika Sellerberg, Diego Di Bartolo, Julia Oberrecht, Jörg C. Tiller, Peter Walzel

The knowledge of enzymatic activity is essential for many industrial processes. The common measurement techniques are time-consuming and therefore cost-intensive. Measurements of viscosities as an indicator for the concentration decay of large molecules are a promising approach for a fast and cheap testing method.

When exposing enzymes to polymeric protein chains, these chains are broken at different places within the molecule. Reduction of chain length, preferably of the long chains leads to significant viscosity breakdown of the said solutions. They then behave similar to solutions with lower polymer concentration, named “apparent concentration”. In reverse, the viscosity decay can be used to characterize the enzyme activity. Besides other quantification standards the characterization of the enzyme activity a is expressed by the obvious reaction rate in e.g. s^{-1}. Assuming the well-known kinetics (Michaelis/Menten) for the reaction at sufficient substrate concentrations and for short reaction time it is valid

$$\partial(c/c_o)/\partial t = -a \qquad (1)$$

with c_o indicating the starting substrate concentration of the protein dissolved after enzyme addition. The slope (-a) stands for the degradation speed shortly after the reaction has started. The concentration of protein polymers at a given molecular weight is linked to the viscosity of the solution. Determination of viscosity provides a cheap and comparative fast approach compared to other methods as calorimetry or spectroscopy due to ordinary relations between apparent substrate concentration and solution viscosity. The apparent concentration can be estimated by the Martin equation in the following implicit form:

$$c = \{([\eta]\cdot \exp_{10}(k_M [\eta]\cdot c)\}^{-1}(\eta) \qquad (2)$$

The intrinsic viscosity is given by $[\eta] = \lim_{c->0} (\eta-\eta_o)/(\eta_o \cdot c)$. The pure solvent has the viscosity η_o , while k_M is the Martin-Parameter available from viscosity measurements and η is the solution viscosity. Equ.(2) must be solved numerically for given data of η.

Water based gelatin-buffer-system gelatin-hydrolysate (ABTEI®-gelatin, M_m=18kg/kmol) could be successfully quantified in terms of protein degradation. The digesting enzyme (Trypsin, Sigma Aldrich®) was used as model enzyme in the degradation experiments. For enzyme concentrations up to 1 mg/ml a linear relationship with respect to enzyme activity has been verified. Fig. 1 shows the viscosity decay vs time for a gelatin solution after enzyme addition.

Fig. 2 shows a fast test device for comparative evaluations of enzymes. The discharge velocity of the solution through the vertical equal sized openings in the right container is higher for the lower viscous enzyme added mixture after given reaction time, compared to the standard gelatin solution with the same concentration in the left container.

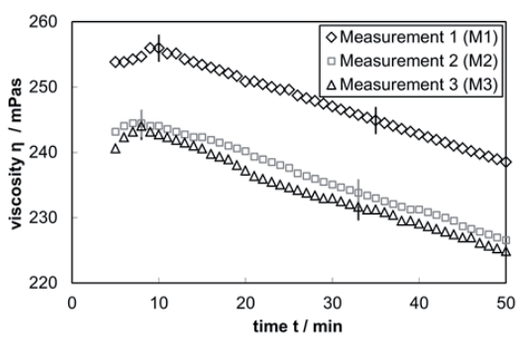

Figure 1: Substrate viscosity vs reaction time in the linear range for c0 = 1200 mg/ml ABTEI®gelatin-hydrolysate in phosphate buffer solution (pH = 7.4) and Trypsin concentration of 1 mg/ml. Relation to starting concentrations/viscosities eliminates variation of data

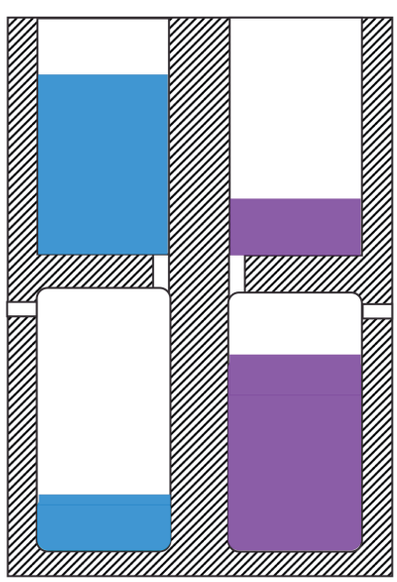

Figure 2: Fast test device for comparison of enzyme activities after and during reaction. The lower viscous enzyme added solution in the upper right container is effusing much faster compared to the one with the standard buffer solution of equal substrate concentration in the right container. Reaction may proceed during the discharge process. Liquid levels indicate relative viscosities

Publications:
M. Sellerberg, D. Di Bartolo, J. Oberrecht, J. C. Tiller, P. Walzel, Viscometric measurement of protease activities on gelatine substrate, Appl. Rheol. 24:6 (2014) 62660; DOI: 10.3933/ApplRheol-24-62660

Contact:
monika.sellerberg@tu-dortmund.de
diego.di-bartolo@bci.tu-dortmund.de
julia.oberrecht@bci.tu-dortmund.de
peter.walzel@bci.tu-dortmund.de

Pattern of conical gas jets and sprays

How do conical jets actually propagate?

Peter Walzel, Johannes Scislowski, Gerhard Schaldach

Hollow conical jets, either single-phase or two-phase, in the latter e.g. water sprays in air, generated by hollow cone nozzles, retain their hollow conical shape only for certain distances. After particular running lengths they reshape into full cone pattern resembling single-phase free jets. The radial relaxation distance of the droplets approximates the starting diameter for the free jet region.

The emerging liquid sheet in the vicinity of the spray nozzle causes conical spread of the drops formed by sheet breakup. Simultaneously the entrained environmental gas passes the spray about perpendicular to the spray propagation and is deflected there into an axial movement inside the spray cone. As soon as the radial velocity component of the droplets is spent due to deceleration of the drops in the environmental gas, the spray pattern is bent inward and reshapes into an axial jet resembling a classical single-phase free jet. Entrainment is the reason for classification of droplets with the larger ones collecting at the outer skirt of the jet and the smaller drops moving inward towards the center of the jet.

The distance as well as the maximum radial expansion of the relaxation area can be approximated assuming low drop Reynolds numbers with the relaxation length of a spherical particle within a stagnant gas:

$$R_{max} = \sin(\Theta/2)\cdot p_f \cdot v_0 \cdot d_{50}^2/18\,\mu_g.$$

Θ is the spray angle, v_0 is the initial velocity, p_f is the density of the fluid and μ_g is the viscosity of the gas and the mass mean diameter of the drops is $d_{50.3}$. Estimated maximum spreading radii exceed measured data by a factor of up to 50% especially for low overhead pressures $\Delta p < 20$ bar, due to neglected swarm behavior. More accurate data are obtained by simulation with CFD as in Figure 2 and have been confirmed with experiments. The following conditions with water are shown: swirl spray nozzle (SCHLICK), nozzle diameter D = 0.6 mm, spray angle Θ = 107°, pressure drop Δp = 30 bar, discharge velocity v_0 = 61 m/s. Mass flow 21.3 kg/h, momentum flux J = 0.36 kgm/s², s. Fig. 1, left.

In contrary, hollow conical gas jets emerging with the same velocity and momentum flux as well as with the same expansion angle as the spray, are practically impermeable for the environmental gas as shown by the smoke strand, (Fig. 1 right). Instead environmental gas is entrained along the cone mantle and is accelerated forming a boundary layer.

After some running length the radial movement fades and a torodial eddy is formed inside the cone with a significant backflow up to the center of the annular slot blocking entrainment of the environmental gas close to the cone axis (Fig. 2 right). A similar pattern is found at the hollow cone spray but only at the very close vicinity to the nozzle where the liquid sheet is still intact. Trials with an annular slot nozzle, width s = 2.1 mm, discharge angle Θ = 108°, discharge velocity v_0 = 62 m/s, air mass flow rate 22 kg/h are shown (Fig. 1 right). The momentum flux was held identical to the spray with J = 0. 36 kg m/s².

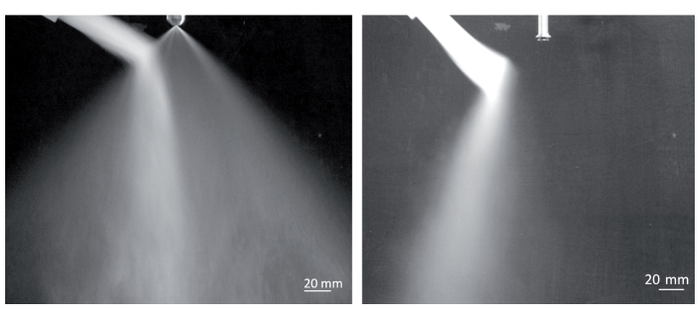

Figure 1: Left: entrainment of smoke strand into the center of a hollow conical spray and deflection into axial direction, right: deflection of smoke strand along the streamlines of a hollow conical gas jet. Photos were taken at equal discharge velocity, mass and momentum flux of both jets, see text.

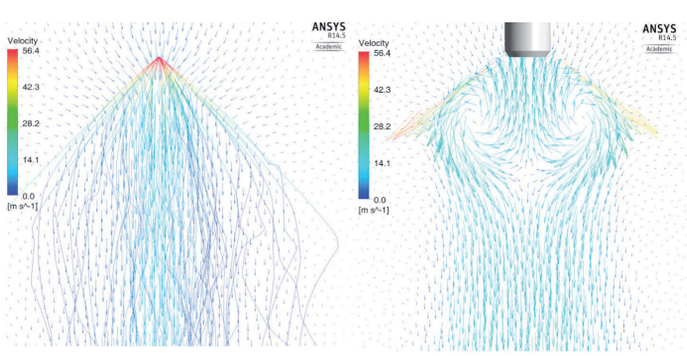

Figure 2: Simulation of gas flow pattern close to the nozzle exits at *identical momentum flux and expansion angle*. Left: hollow conical spray jet. Right: hollow conical gas jet

Contact:
peter.walzel@bci.tu-dortmund.de
johannes.scislowski@bci.tu-dortmund.de
gerhard.schaldach@bci.tu-dortmund.de

Fluid Mechanics (SM)

Spreading of liquid droplets

Experimental study of liquid droplets spreading on horizontal rotating plates

Mirja Blank, Peter Ehrhard

The spreading of liquid films is involved in many coating processes, e.g. in the spin-coating process. To achieve a high quality of the coating, the spreading liquid layer should be thin and homogeneous. Instabilities at the wetting front may lead to an inhomogeneous thickness of coating layer and to uncoated areas. An analytical model for the dynamic spreading of axisymmetric droplets on resting substrates has been derived by Ehrhard & Davis (1991). By invoking lubrication approximation, an analytical solution is derived, valid in the limit of small capillarity numbers (C → 0). Boettcher (2014) extends this model to include a rotating substrate and, moreover, presents a linear stability analysis for the initially axisymmetric droplets. The aim of the present experiments is to validate the model of Boettcher (2014).

Perfectly wetting silicone oil droplets are applied onto rotating glass plates. A Schlieren system is set up to observe the wetted area and a chromatic confocal distance sensor is used to measure the contour of the droplet. This sensor is mounted on a crossbar and is traversed radially across the rotating droplet through its center. The sensor gathers information at up to 2 kHz along that line. It measures the distance from the sensor to the liquid/gas interface. By subtracting the initially-measured level of the rotating plate, the contour of the droplet can be derived.

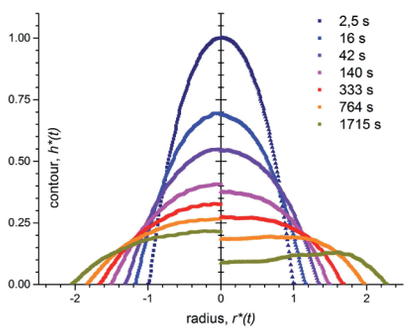

Figure 1: Contours of droplet in time, non-rotating substrate (left) and rotating substrate (right, rotation rate Ω_1).

Figure 1 shows the evolution of two different droplets. On the left side, the spreading on a non-rotating plate is shown. On the right hand side, a droplet with a similar volume is shown, but the plate rotates at $\Omega_1 = 4\pi$ 1/s. The height $h^*(t)$ is scaled with the initial height at the center of the droplet $h_0 \approx 0.3$ mm and the radius $r^*(t)$ is scaled with the initial radius $r_0 \approx 2.5$ mm. Initially, both droplets spread similarly. After about 100 s, the height at the center of that rotating droplet decreases faster, if compared to the non-rotating case. The development of a so-called capillary ridge can be observed after about 1700 s. The characteristic of such a capillary ridge is that the maximum height of the spreading layer appears at an annular ring and not at the center of the droplet.

For even higher angular velocities, the capillary ridge moves radially outwards and first instabilities start to develop. Therefore, the rotationally-symmetric contour of the droplet does not persist. As the chromatic confocal sensor traverses along a straight line with the droplet rotating below, it becomes difficult to infer contours from the gathered data for non-axisymmetric cases. Nevertheless, the Schlieren images capture the footprint of the droplet also for such non-axisymmetric cases and, thus, allow characterize the modes of instability.

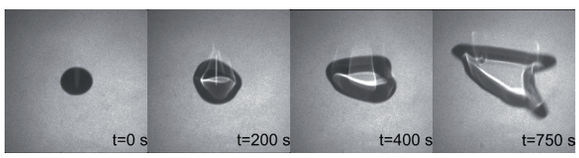

Figure 2: Development of an instability for a droplet rotating at Ω_2.

Figure 2 shows the development of fingers as consequence of an instability. The droplet starts with a circular footprint. The rotation rate is constant at $\Omega_2 = 8\pi$ 1/s. Its footprint appears already distorted at 200 s. As time develops, three dominant fingers grow out of the contact line. The mode of instability appears to be $k = 3$. Later, some not yet fully-developed fingers are visible at 750 s.

The experimental data up to now do not show the basic modes in pure form. Instead, a superposition of several basic modes can be observed.

Contact:
mirja.blank@bci.tu-dortmund.de
p.ehrhard@bci.tu-dortmund.de

Publications:
Boettcher, K.E.R.; Ehrhard, P. (2014), Europ. J. Mech. B/Fluids. **43**, 33-44
M.Blank, P. Ehrhard, Fachtagung „Lasermethoden in der Strömungsmesstechnik“. (GALA) **13**, 2012.

Technical Biochemistry (TB)

In silico profiling of *Escherichia coli* and *Saccharomyces cerevisiae* as terpenoid factories

An analysis of the most prominent heterologous hosts

Evamaria Gruchattka, Verena Schütz, Oliver Kayser

Our focus was set on the in silico analysis of metabolic networks of the most prominent heterologous hosts E. coli (gut bacterium) and S. cerevisiae (baker's yeast) relating to the efficient supply of isopentenyl diphosphate (IPP). IPP is the common terpenoid precursor, which is produced by the microbes themselves naturally. Microbes producing IPP in high amounts are a prerequisite to produce plant terpenoids efficiently.

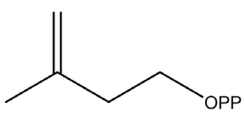

Figure 1: Isopentenyl diphosphate (IPP).

Terpenoids are a class of natural products with important medicinal and industrial applications from drugs (artemisinin, paclitaxel) to biofuel precursors (bisabolene, farnesene) to flavor compounds (patchoulol, linalool, menthol, eucalyptol).

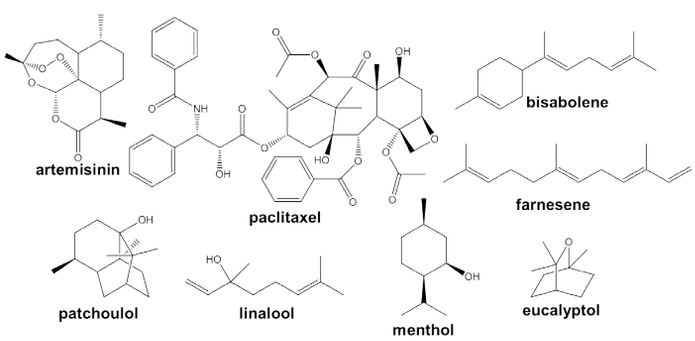

Figure 2: Diversity of terpenoids.

Several of these bioactive compounds are scarce and produced only in low amounts in plants, which makes the production in plants uneconomical and environmentally destructive. The total chemical synthesis of many terpenoids is challenging due to their complex structure and neither ecologically nor economically efficient. Alternatively, the use of a microbial platform organism for the production of terpenoids may offer the possibility of large-scale, cost-effective and environmentally friendly industrial production independent from climate or cultivation risks.

Today, *E. coli* and *S. cerevisiae* are the most widely used microorganisms for heterologous terpenoid production but terpenoid yields are still low. Thus, the aim of this study was to identify new metabolic engineering targets for an enhanced terpenoid yield.

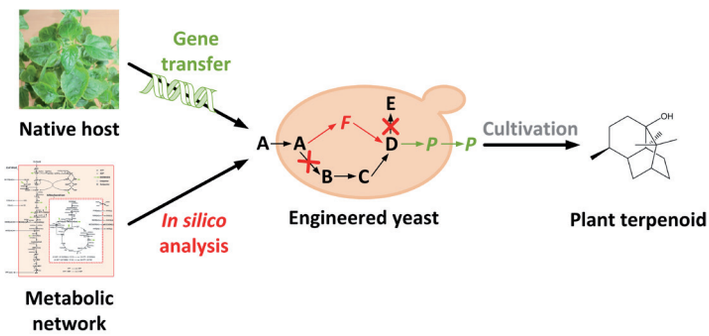

Figure 3: Schematic representation of the approach. First, terpenoid genes have to be transferred from the plant to the microbial host (*E. coli or S. cerevisiae*) to be able to produce plant terpenoids in microbes. Second, the metabolic network of the microbes is analyzed *in silico* to identify targets for metabolic engineering of the microbial host for an enhanced terpenoid biosynthesis.

E. coli and *S. cerevisiae* use different pathways to supply IPP. The analysis of the metabolic networks revealed that the DXP pathway of *E. coli* has theoretically, based on stoichiometry, a higher potential to produce IPP in high yields than the one of yeast. Moreover, non-fermentable carbon sources have a higher potential for the production of terpenoids in high yields in comparison to sugars.

Deficiencies in energy and redox equivalents are identified in the metabolic networks and are a basis for metabolic engineering strategies. Different knockout and heterologous overexpression strategies are presented leading either to increased minimal or to an enhanced theoretical maximum terpenoid yield on different carbon sources. [1,2]

Contact:
Evamaria.Gruchattka@bci.tu-dortmund.de
Oliver.Kayser@bci.tu-dortmund.de

Publications:
[1] Gruchattka E, Hädicke O, Klamt S, Schütz V, Kayser O: **In silico profiling of *Escherichia coli* and *Saccharomyces cerevisiae* as terpenoid factories**. Microb Cell Fact 2013, **12**:84.

[2] Abstracts of the 26th International Conference on Yeast Genetics and Molecular Biology. Frankfurt/Main, Germany. August 29-September 3, 2013. Yeast 2013, **30 Suppl** 1:S22-253.

Endophytes as antivirulence agents

Strategies employed by endophytes for maintaining host tissue colonization and aiding host plant defense

Parijat Kusari and Oliver Kayser

Surviving of endophytes is a battle with chemical compounds and using these tactics we may develop new antibiotic therapy strategies. Quorum sensing is an interesting concept in nature by endophytes that can be translated in future drug discovery concepts. This study exemplifies a significant biological role played by the endophytes in different ecological niches, by acting as antimicrobial agents, not only aiding host plant defense but also for teaching us new ways for natural product drug discovery.

"Endophytes" are a diverse group of microorganism inhabiting the internal tissues of the plant and constantly co-evolving with the host plant and associated microorganisms. These multitudinous interactions enable the endophytes to counter the invasion by a plethora of generalist and specific pathogens. Therefore, in order to maintain colonization inside the host plant in different ecological niches, endophytes employ certain functional traits developed during the course of evolution. Our work emphasizes on one such trait, commonly known as "quorum quenching".

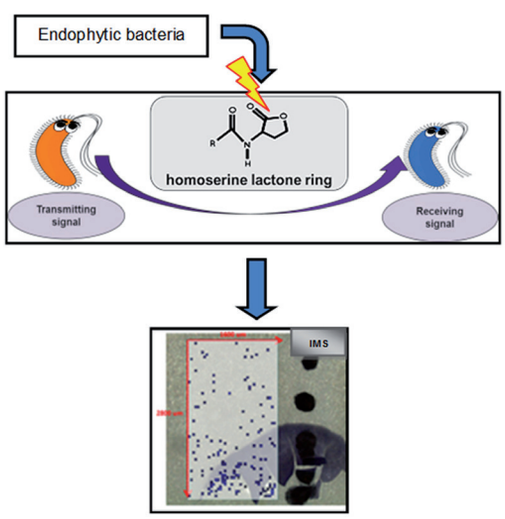

Figure 1: Schematic representation of quenching of quorum coordination by bacterial endophytes of *Cannabis sativa* L

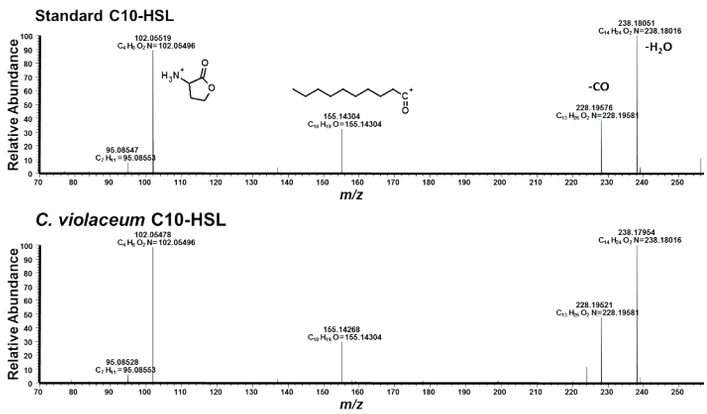

Figure 2: Representative MS/MS spectra showing comparison of C10-HSL in authenticated standard (top) and in the control biosensor strain (bottom)

Our previous work on the attack-defense-counter-defense strategies of the endophytic fungal community revealed their potential as biocontrol agents. Therefore, we further our investigation to study the ecological context of the bacterial endophytes in providing host fitness benefits. In this study, we use a combination of high performance liquid chromatography high-resolution mass spectrometry (HPLC-ESI-HRMs) and matrix assisted laser desorption ionization imaging high-resolution mass spectrometry (MALDI-imaging-HRMS) to quantify and visualize the selective and differential quorum quenching capability of potent bacterial endophytes harbored in *Cannabis sativa* L. plants.

Our work provides fundamental insights into the potential of endophytic bacteria as biological tools for biocontrol of phytopathogens and as antivirulent agents both within the ecological context and clinical settings.

Publications:
[1] Kusari P., Kusari S., Lamshoeft M., Sezgin S., Spiteller M., Kayser O. (2014) Quorum quenching is an antivirulence strategy employed by endophytic bacteria. **Applied Microbiology and Biotechnology. Accepted**

[2] Kusari P., Spiteller M., Kayser O., Kusari S. (2014) Recent advances in research on Cannabis sativa L. endophytes and their prospect for the pharmaceutical industry. In: Kharwar R.N. et al. (eds.) **Microbial Diversity and Biotechnology in Food Security**, Springer. In Press.

[3] Kusari P., Kusari S., Spiteller M., Kayser O. (2013) Endophytic fungi harbored in *Cannabis sativa* L.: Diversity and potential as biocontrol agents against host plant-specific phytopathogens. **Fungal Divers** 60:137-151

Contact:
Parijat.kusari@bci.tu-dortmund.de
Oliver.kayser@bci.tu-dortmund.de

Collaborators:
Souvik Kusari (s.kusari@infu.tu-dortmund.de) and Michael Spiteller (m.spiteller@infu.tu-dortmund.de),
Institute of Environmental Research (INFU), Department of Chemistry and Chemical Biology of TU Dortmund

Technical Chemistry (TC)

Catalysis with Pd-nanoparticles

A new protocol to synthesize dihydrodicyclopentadienes via mono hydrogenation

Arno Behr, Adrian Lux

With the use of Pd-nanoparticles dihydrodicyclopentadienes (DHDCP) can be synthesized under mild reaction conditions. Thereby dicyclopentadiene (DCP) as raw material is in a mono hydrogenation transferred into the products. At low temperatures of 50 °C and a hydrogen pressure of only 5 bar it is possible to achieve a high conversion of up to 85 %. The ratio between the DHDCP and the full hydrogenated tetrahydrodicyclopentadiene (THDCP) can be shifted from 1 : 8 to 7 : 1 by variation of the reaction conditions. After the reaction an easy isolation of the products and good recycling of the nanocatalyst is possible.

Dicyclopentadiene can be hydrogenated to more valuable products, the two different dihydrodicyclopentadienes (**2a** and **2b**) and tetrahydrodicyclopentadiene (**3**). DCP is easy available, because it is an important component of the C_5-fraction of the steamcracker.

For the more valuable DHDCP are industrial processes known, e.g. as comonomer in polymerization reactions or as a starting material for flavor production. THDCP is used in the production of jet fuels or adamantane.

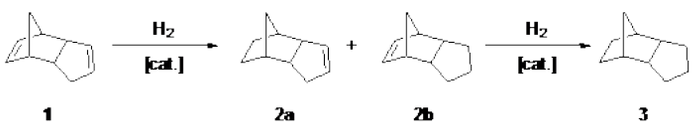

Figure 1: Synthesis of dihydrodicyclopentadienes (DHDCP, **2a** and **2b**) and tetrahydrodicyclopentadiene (THDCP, **3**)

For the synthesis of DHDCP a known synthesis route is the hydrogenation of protected norbornene. But this reaction sequence is not favorable for industrial processes.

Based on the experiments in the working group of A. Behr, which shows selectivity effects of nanoparticles-catalysts in hydrogenation reactions, we investigated the hydrogenation of DCP with the aim getting the mono-hydrogenation products.

During our experiments we have observed an influence of the solvent, the temperature and hydrogen pressure on the product mixture of the reaction. For example in cyclopentanone as solvent only the formation of **3** was observable. If we used propylene carbonate the monoolefines **2** could be synthesized with selectivity's up to 87 %.

At low hydrogen pressure high amounts of product **2** are possible. Also if we worked at room temperature the product **2** could be obtained with up to 95 %, but with a conversion from only 45 %. Also longer reaction times of 8 or more hours (instead of 2 hours) are required.

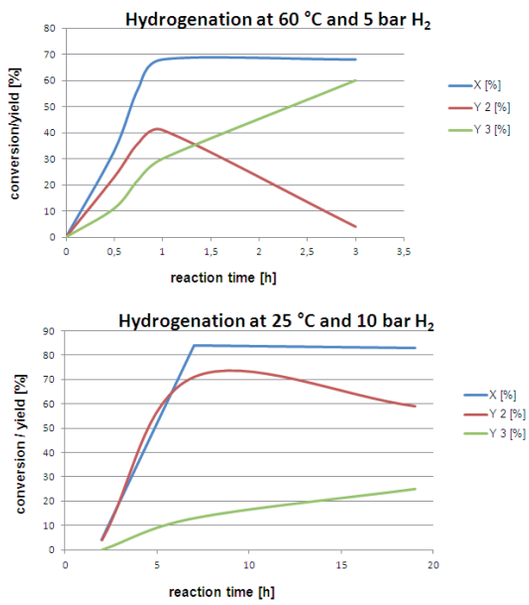

Figure 2: Conversion-time plots for different reaction conditions

An easy recycling of the catalyst solution is possible. For this purpose first the insoluble solid products was separated by filtration. After that the remaining catalyst solvent solution can directly reuse in a next run. But it is possible that the selectivity decreases drastically. To prohibit this effect, the catalyst solution can be regenerated between the runs, by stirring the catalyst solution for 2 hours at 80 °C under hydrogen.

Contact:
adrian.lux@udo.edu
arno.behr@bci.tu-dortmund.de

Publications:
A. Behr, V. Manz, A. Lux, A. Ernst, "Highly selective mono-hydrogenation of dicyclopentadiene with Pd-nanoparticles", Catal. Lett. 2013, 143 (3), pp. 241-245, doi:10.1007/s10562-013-0960-3

Epoxidation of methyl oleate in an aqueous biphasic medium

An efficient reaction protocol for the recycling of a homogeneous oxidation catalyst

Nils Tenhumberg, Arno Behr

The epoxidation of methyl oleate was performed under single phase and biphasic conditions utilizing molybdenum trioxide as catalyst and tert. butyl hydroperoxide as oxidant. Under optimized reaction conditions, the 9,10-epoxy stearic acid methyl ester was obtained in nearly quantitative yields. The recycling of the homogeneous catalyst was performed by immobilization of the catalyst in an aqueous biphasic solvent system using water soluble ligands

Epoxidised plant oils and fatty acid derivatives are used in various applications in chemical industry. They are applied as plasticisers and as starting material for epoxy resins. Commercially available epoxidised fatty acids are typically produced using peroxy acids as oxidant. However, because of the known disadvantages of this process (hazardous handling of peracids in large quantities, formation of undesired by-products) the development of new catalytic reaction protocols is still an important subject of research interest.

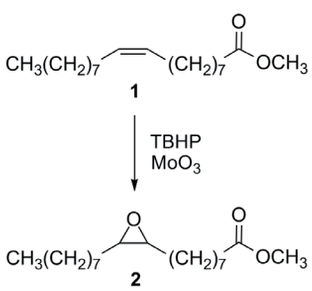

Figure 1: Epoxidation of methyl oleate **1**

In our initial investigations we found that the homogenous epoxidation of methyl oleate **1** could be obtained within excellent yields up to 96% utilizing molybdenum trioxide (MoO_3) as catalyst and *t*-butyl hydroperoxide (TBHP) as oxidant under single phase conditions (Figure **1**).

In order to solve the challenging issue of the separation and the recycling of the homogeneous catalysts the reaction was performed in an aqueous biphasic solvent system. The immobilisation of the catalyst in a liquid/liquid biphasic system represents a smart technology for the recycling of a homogeneous catalyst which combines both the high flexibility of the homogeneous catalysts and the simple separation of the catalysts from the product.

In this work the homogeneous molybdenum catalyst was immobilised in an aqueous biphasic solvent system (water/*p*-xylene) using commercial available water soluble sodium triphenylphosphine trisulfonate (NaTPPTS) or dimethylformamide (DMF) as ligands (Table 1). After the reaction the aqueous catalyst solution was easily separated from the organic product by phase separation and could be reused. During catalyst recycling no remarkable change of the selectivity of the reaction was observed. Only a low decrease of the activity of the catalyst was noticed. Also in the third runs good yields of 73% and 71% were obtained, respectively. Especially with DMF as ligand a very low catalyst leaching of 1 ppm was achieved in all runs.

Table 1. Catalyst recycling

Catalyst	RUN	Conv. 1 [%]	Yield 2 [%]	Mo-Leaching[b] [ppm]	[%]
MoO_3/NaTPPTS	1	95	89	10	2.0
	2	91	82	7	1.4
	3	78	73	3	0.6
MoO_3/DMF	1	91	89	1	0.2
	2	78	76	1	0.2
	3	74	71	1	0.2

Reaction conditions: 5 mmol methyl oleate **1**, 0.05 mmol MoO_3, 0.025 mmol ligand, 10 ml solvent (*p*-xylene:H_2O = 9:1), 15 mmol TBHP (70% aq), 138°C, 6 h. [b] Limit of quantitation: 5 ppm. Conv. = Conversion.

Moreover this reaction protocol represents a simple reaction procedure for the recycling of a homogeneous oxidation catalyst employing an aqueous/organic biphasic system.

Contact:
arno.behr@bci.tu-dortmund.de

Financial support by BMELV in cooperation with Emery Oleochemicals GmbH

Publications:
N. Tenhumberg, A. Behr, in preparation

Hydroamination of β-myrcene and catalyst recycling by TMS

Continuous production of terpenyl amines in a Taylor-Couette reactor

Tobias Färber, Arno Behr

The hydroamination of myrcene with morpholine was investigated in a batch reactor in laboratory scale and a continuously operated Taylor-Couette reactor (TCR) in miniplant scale. The recycling of the valuable palladium catalyst is achieved by thermomorphic solvent systems (TMS).

The renewable resource β-myrcene, which can be derived from a by-product of the paper industry, offers the easy access to alkyl amines based on renewables. The hydroamination of myrcene with the conveniently accessible amine morpholine (Figure 1) is catalysed by a palladium complex. The catalytic system consists of the palladium precursor $Pd(CF_3CO_2)_2$ and the ligand diphenylphosphino-butane (DPPB).

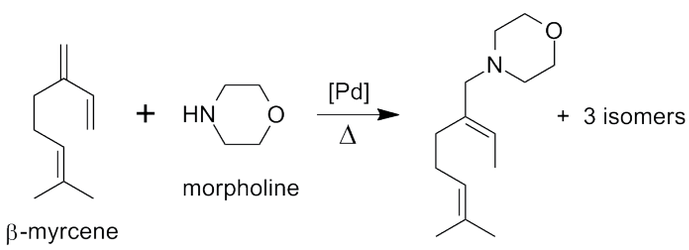

Figure 1: Hydroamination of β-myrcene

The reaction is carried out in a thermomorphic solvent system (TMS) with a temperature-dependant miscibility gap. The system consists of acetonitrile and *n*-heptane, which enables the recovery of the valuable metal catalyst. At reaction temperature the system is homogenous (no mass transfer limitation), at separation temperature the system is biphasic (catalyst separation). The catalytic system is dissolved in the polar acetonitrile phase, the non-polar products in the heptane phase. Thus the products can be separated from the catalyst and the catalytic phase can be recycled.

After tailoring an efficient catalyst and TMS system on the laboratory scale, the hydroamination was transferred into a continuously operated Taylor-Couette reactor in miniplant scale. This reactor type combines the benefits of a CSTR (ideal mixing) with the advantages of a PFR (plug flow behavior) thus enabling the efficient catalysis of the hydroamination at high yields (Figure 2). The constructed reactor is equipped with an efficient double jacketed heating system as well as a redundant sealing system by graphite-filled Teflon seals.

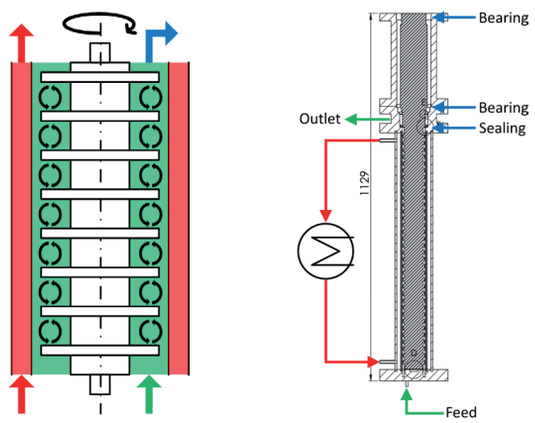

Figure 2: Principle and technical drawing of the Taylor-Couette reactor (TCR) for continuous hydroamination

The reactor was integrated into a miniplant and tested in the continuous hydroamination (Figure 3).

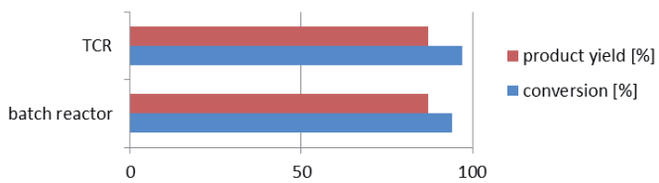

Figure 3: Hydroamination in batch and continuous TCR

The last step is the integration of the TCR into the miniplant concept. Figure 4 shows a simplified version of the process flow chart without the process control systems.

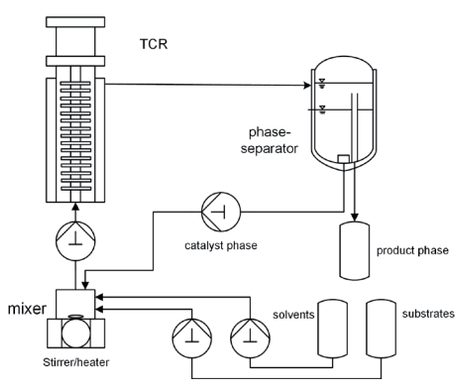

Figure 4: Miniplant with TCR and catalyst recycling

SusChemSys is co-financed by the Regional Development Fund -investing in your future- of the European Union and the state of North Rhine-Westphalia

Contact:
arno.behr@bci.tu-dortmund.de

Publications:
[1] Poster Jahrestreffen Deutscher Katalytiker, Weimar, 2014

First rhodium catalyzed hydroformylation of cyclopentadiene

Selective access to cyclopentadiene aldehydes

Denys Levikov, Dennis Vogelsang, Arno Behr

Here we present the first rhodium catalyzed hydroformylation of cyclopentadiene (CP) leading to cyclopentane carbaldehydes. Under mild reaction conditions of 100 °C and 30 bar synthesis gas with use of tertiary amines as co-catalysts yields up to 65 % of cyclopentane carbaldehyde 3 and 11 % of cyclopentane dicarbaldehyde 4 were achieved in a reaction time of 3 hours.

Cyclopentadiene (CP) **1** and dicyclopentadiene (DCP) **2** are important components in the C5-fraction of the steamcracker. Typically, 25 weight% of the C5-fraction are cyclopentadiene, which separation is carried out by dimerization of CP to DCP (Figure 1).

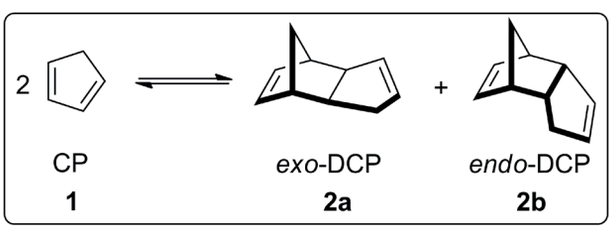

Figure 1: Dimerization of cyclopentadiene to dicyclopentadiene

The latter can be cracked again to CP by a retro-Diels-Alder reaction [1]. Cyclopentadiene itself is stable only over a short period at -80 °C. Therefore, only a few industrial applications for cyclopentadiene are known [2].

The mono- and dialdehydes of cyclopentadiene can be used in different areas of the chemical industry, e.g. as building blocks for polymers, as well as fragrances. Hence, the dimerization process is observed as a side reaction in every homogeneously catalyzed reactions starting from CP. Therefore, the desired reaction, e.g. hydroformylation, has to be faster than the competitive dimerization process.

So far it was not possible to suppress the formation of DCP in hydroformylation completely. To the best of our knowledge the first successful hydroformylation of cyclopentadiene was investigated by Adkins and Williams in 1952. Hence, cyclopentane carbaldehyde 3 was obtained as a main product in cobalt catalyzed hydroformylation with 37 % yield at 145-155 °C and 255 bar synthesis gas [3].

We have successfully studied the rhodium catalyzed hydroformylation of CP lowering the harsh reaction conditions to 100 °C and 30 bar synthesis gas. The key of success is the use of tertiary amines, e.g. triethylamine, in order to reduce dimerization. Also we have found that ligands with small bite angle lead to DCP-products and with big bite angle over 120° to **3** & **4**. The formation of **3** is a result of a tandem reaction, which consists of selective hydrogenation of CP to cyclopentene and subsequent hydroformylation to the saturated monoaldehyde (Figure 2).

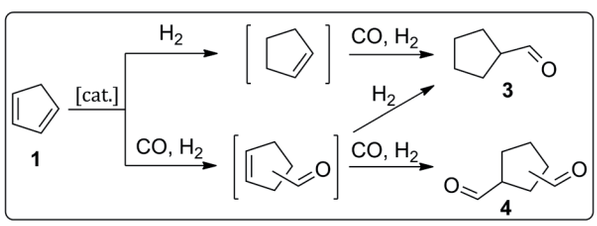

Figure 2: Possible reaction pathways in the hydroformyla-tion of CP for formation of **3** & **4**

With rhodium catalyst yields up to 65 % of **3** and 11 % of cyclopentane dicarbaldehyde **4** were achieved in a reaction time of 3 hours. This is the first successful rhodium catalyzed hydroformylation of cyclopentadiene giving **3** and **4** as main products in moderate yields.

[1] Hönicke, D., Födisch, R., Claus, P., Olson, M., "Cyclopentadiene and Cyclopentene", Ullmann's Encyclopedia of Industrial Chemistry, Wiley, 7th edition, electronic release, 2008.

[2] Behr, A., Manz V., Erdöl Erdgas Kohle, 2011, 10, 366.

[3] Adkins, H., Williams, J. R., J. Org. Chem., 1952, 17, 980.

Publications:
D. Levikov, D. Vogelsang, A. Behr, First rhodium catalyzed hydroformylation of cyclopentadiene. Poster: *47. Jahrestreffen Deutscher Katalytiker*, Weimar, **2014**

Contact:
arno.behr@bci.tu-dortmund.de

Financial support from the Deutsche Forschungsgemeinschaft (DFG) is gratefully acknowledged

Self metathesis of fatty acid methyl esters

An efficient way to difunctional substrates for polymer synthesis

Arno Behr, Stephanie Toepell

Fats and oils represent the largest share of natural resources with 40% in chemical industry. Of particular interest is the metathesis of unsaturated oleochemicals. It is an excellent tool for generating α,ω-difunctional substrates, which are useful intermediates for polymer synthesis. A systematic investigation and a comparison of different oleochemical compounds as starting materials are therefore of great scientific interest. By varying the oleochemical substrate different chain length of the bifunctional products can be generated.

The specific reaction conditions in the self metathesis of methyl oleate, methyl undecenoate, methyl erucate and methyl ricinoleate were optimized for high conversions in combination with high selectivities to the primary metathesis products. (Fig. 1)

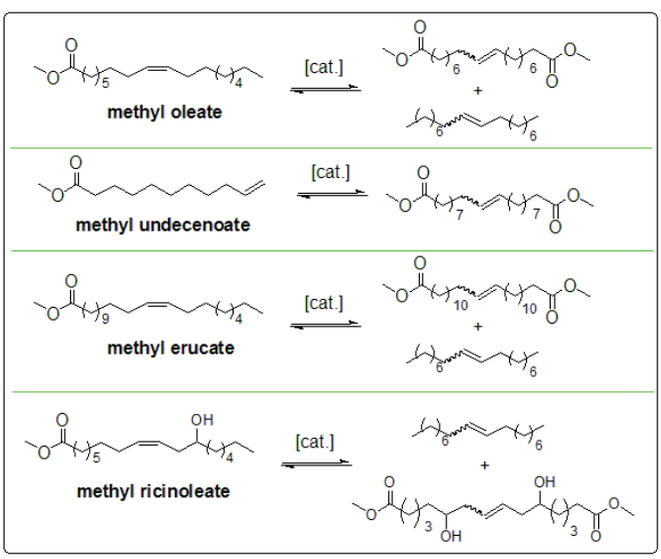

Figure 1: Self metathesis of different fatty acid methyl esters to their primary metathesis products

We examined the following reaction conditions in the optimizations of the individual oleochemical self metathesis: screening of various homogeneous Ruthenium-metathesis catalysts, catalyst concentration, temperature, time, solvents and the substrate/solvent-ratio. The impact of the specific conditions on the individual reaction system was investigated and concerned.

With the innerstanding fatty substrates a maximum yield of the products of 50% is possible due to the equilibrium of the reactions. A clear trend of chain length and functionalization in the fatty chain could be detected.

The hydroxyl group in the methyl ricinoleate lead to a longer reaction time and a higher amount of needed catalyst. It is possible to counteract this effect by introduction of a hydroxyl-protection group. This approach lead to a lower viscosity of the substrate and therefore to an increased reactivity in self metathesis.

The higher chain length in methyl erucate shows an influence of the substrate concentration to the reaction time and temperature. In this case a temperature of 80 °C is necessary in order to compare the results with methyl oleate.

When using the endstanding methyl undecenoate nearly 100% of the C20-diester can be achieved by applying vacuum to continuous removing the also resulting ethene. Thereby a reaction time of only 15 minutes is sufficient.

By choosing the right reaction conditions, we obtain quantitative yields with all types of investigated fatty acid methyl esters. Very mild reaction conditions (temperatures: 20 – 80 °C, reaction times: 15 minutes – 3 hours) and the use of a small amount of commercial available catalyst (0.25 mol% based on the fatty acid methyl esters) are sufficient for this results. The described oleochemical self metathesis can be handled at air without loss in activity. Also any solvents of analytical standard can be used without the need of previous purification. In all cases only the primary metathesis products are formed without any isomerization products.

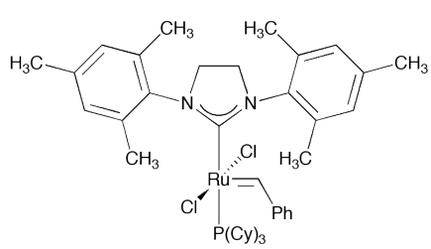

Figure 2: Grubbs catalysts are a very efficient in self metathesis catalysts

Contact:
arno.behr@bci.tu-dortmund.de

Financial supported by BMELV in cooperation with Emery Oleochemicals GmbH

Rhodium-catalyzed codimerization of n-butenes with allylic halides

A simple reaction procedure for the production of long chained alkenes

A. Behr, Z. Bayrak (TU Dortmund), S. Peitz, D. Maschmeyer, G. Stochniol (Evonik Industries)

This article describes the codimerization of n-butenes with allylic halides such as cinnamyl chloride and crotyl chloride. The highly active catalyst $RhCl_3 \cdot 3H_2O$ was investigated, resulting 44% yield of codimers with cinnamyl chloride and 1 butene. The oligomerization of alkenes, especially ethene, propene and butenes has been studied quite extensively. Most of the investigated catalyst systems consist of a transition metal complex of metals like nickel, palladium, chromium, titanium and rhodium. The catalyst selection depends on which alkene is used and on the desired product. Cramer et al. demonstrated that $RhCl_3 \cdot 3H_2O$ is a very active cooligomerization catalyst for dienes and alkenes. Recent research by Behr et al. has demonstrated that it is also possible to cooligomerize ethene with conjugated linoleic acids, an oleochemical diene. [1-3]

Now, we have investigated for the first time that allylic halides can also be codimerized with alkenes such as 1 butene and $RhCl_3 \cdot 3H_2O$ as a catalyst precursor. The postulated mechanism for the codimerization of 1-butene with crotyl chloride is described in Figure 1. In the first step, the rhodium hydride is reduced to a rhodium (I) complex by releasing HCl (step **A**). The crotyl chloride leads to a reoxidation to rhodium(III) via an oxidative addition (step **B**). Then a 1-butene molecule is bound to the rhodium center (step **C**). Instead of a ß-hydride elimination in step **D**, an insertion of the crotyl ligand between rhodium and 1-butene occurs. The catalytic active rhodium hydride and the codimer may be generated after a ß-hydride elimination (step **E**).

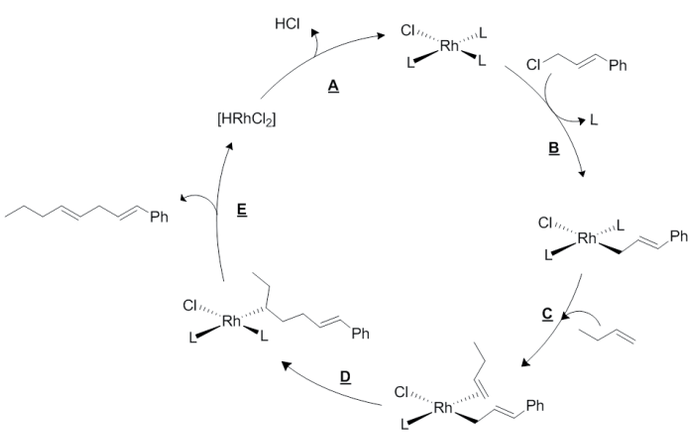

Figure 1: Postulated mechanism of the codimerization of crotyl chloride with 1-butene.

Different allylic halides were used to codimerize with 1-butene in order to define what kind of allylic halides react with 1-butene. For this purpose, we ran reactions with allyl chloride, crotyl chloride, crotyl bromide and cinnamyl chloride, yielding the codimers **1** to **4**. The codimer yields of **4** to **4** represent the total yield of the isomers in each box (Figure 2). Both isomers are formed in each reaction, but could not be separated by GC.

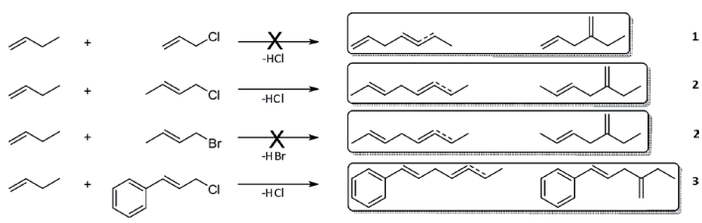

Figure 2: Reactions of 1-butene with allylic halides.

The results in Table 1 show that the reactions with 1 mol% of $RhCl_3 \cdot 3H_2O$ only led to a product formation for crotyl chloride and cinnamyl chloride, where the codimerization of cinnamyl chloride and 1 butene yielded a maximum yield of 44% of the codimers. Additionally, an increasing yield of the codimers was observed with larger alkyl chains in the allylic position of the educt. This can be explained by the postulated mechanism in which an allylic rhodium species is formed in step **B** (Figure 1). The allylic anion can be stabilized most effectively by a benzyl chain, due to its resonance stabilization.

Table 1: Results of the allylic compound screening.

catalyst	allylic compound	$Y_{codimer}$ / %
$RhCl_3 \cdot 3H_2O$	crotyl bromide	0
$RhCl_3 \cdot 3H_2O$	allyl chloride	0
$RhCl_3 \cdot 3H_2O$	crotyl chloride	12
$RhCl_3 \cdot 3H_2O$	cinnamyl chloride	44

(m(1,4-dioxane)/m(1-butene)=5, c(cat.)=1 mol%, T=70 °C, 750 rpm, t=18 h , y: based on n(1-butene))

Contact:
arno.behr@bci.tu-dortmund.de

[1] A. Behr, Angewandte homogene Katalyse, Wiley-VCH (Weinheim) 2008.
[2] H. Witte, Entwicklung, Projektierung und Untersuchung eines kontinuierlichen Miniplantverfahrens zur Herstellung verzweigter Fettstoffe, Dissertation TU Dortmund, 2013.
[3] Q. Miao, Rhodium catalyzed cooligomerization of ethylene with conjugated dienes, Dissertation TU Dortmund, 2006.

Financial support by Evonik Industries

Publications:
A. Behr, Z. Bayrak, S. Peitz, D. Maschmeyer, G. Stochniol, *'Rhodium catalyzed codimerization of n-butenes with allylic halides'*, App. Cat. A, 2014, 476, pp. 68-71

Characterizing Electrochemical Oxygen Reduction Reaction (ORR)

A new contribution to old questions, used to save energy in chlor-alkali electrolysis

Gregor Damian Polcyn, Jens Wilhelm Kuhlmann, Jakob Jörissen

Up to 30 % saving of electrical energy in chlor-alkali electrolysis is possible if the common hydrogen evolution is replaced by oxygen consumption in an Oxygen Depolarized Cathode (ODC), as it is used in fuel cells. This is corresponding to much energy since electrochemical production of chlorine and caustic soda is worldwide one of the biggest consumers of electricity (in Germany 4 % of total electrical power). The process using ODC´s is industrially realized in the Bayer MaterialScience AG – leading partner in a research project of companies and universities, including TU Dortmund, funded by Bundesministerium für Bildung und Forschung (BMBF). Improvement and optimization require a better understanding of ODC and ORR. Interesting new knowledge was obtained by current interruption measurements.

The electrochemical Oxygen Reduction Reaction ORR, carried out in an Oxygen Depolarized Cathode ODC, is complex and difficult to describe. The high overpotential of ORR using available catalysts is responsible for large energy efficiency losses of fuel cells. In spite of long lasting research and great interest in science and industry there are different unresolved questions.

An old method from 1943, but with new technical possibilities of fast switching MOSFET transistors as well as high-speed / high-resolution data acquisition, was used to characterize ORR / ODC: current interruption measurement. It was adapted to electrolysis cells for laboratory (3 cm² ODC area, 'half cell' only with caustic soda electrolyte, see Fig. 1) and pilot plant (100 cm² ODC area, full chlor-alkali electrolysis).

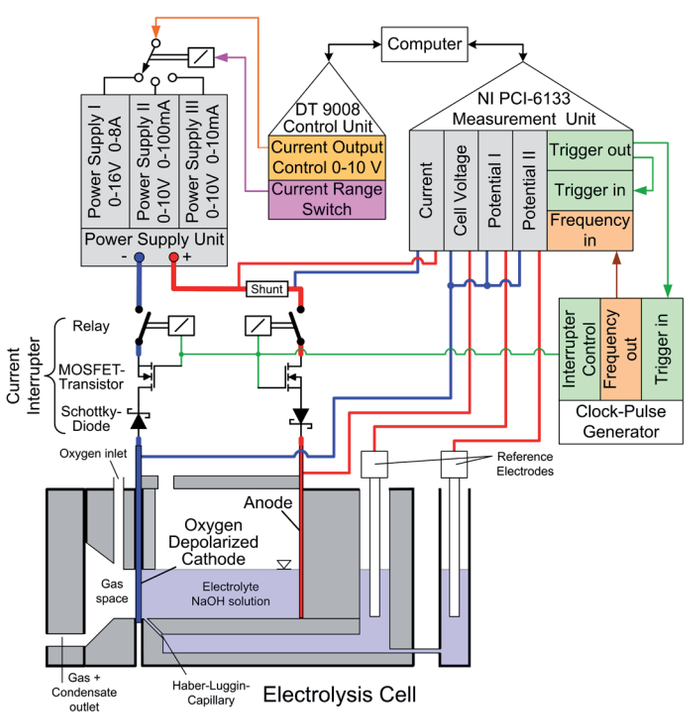

Figure 1: Setup for current interruption measurements

The setup in Fig. 1 enables automatized electrolysis and shutting down within ca. 1 µs. The ODC potential is recorded as the sum of equilibrium potential and overpotentials. Data acquisition uses a decreasing clock rate for displaying the overpotential relaxation curve (black diamonds in Fig. 2) from 1 µs to 100 s (logarithmic time scale in eight decades which allows to show the slew rates).

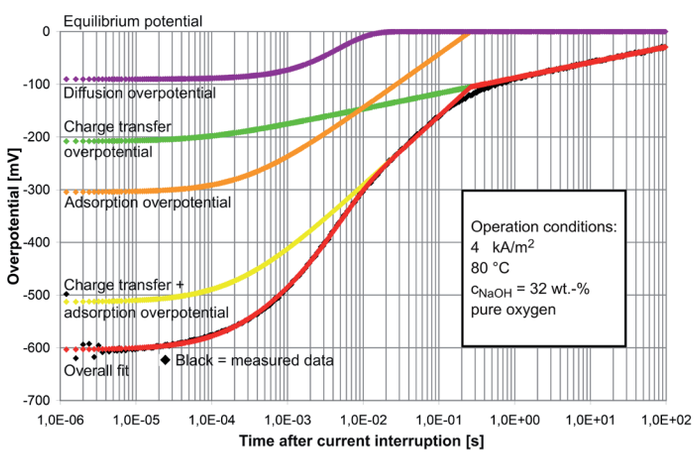

Figure 2: Overpotential relaxation curve of an ODC

During operation the double layer capacity of the ODC is charged up to the sum of overpotentials (here – 600 mV). After interrupting the external cell current this charged capacity is supplying a continued internal current flow for ORR until the equilibrium potential is reached. The different overpotentials – of charge transfer, adsorption, diffusion – decrease with characteristic slew rates. They are distinguished by curve fitting (overall fit = red diamonds in Fig. 2) and described using a new model. It characterizes an ODC based on only one measurement.

Contact:
jakob.joerissen@bci.tu-dortmund.de

Publications:
In preparation for
Journal of Applied Electrochemistry / Electrochimica Acta

Highly selective dimerization and trimerization of isobutene

Linearly linked products of isobutene are accessible using homogeneous Ni-catalysts

Nils Rentmeister, Thomas Seidensticker, Jonas Vosberg and Arno Behr

The unique linear linkage of isobutene to generate high valuable C8-precursors for plasticizers is feasible using special nickel catalysts. (4-Cyclooctene-1-yl)(1,1,1,5,5,5-hexafluoro-2,4-acetylacetonato)nickel as well as aluminum alkyl activated nickel acetylacetonates produce isobutene dimers with high selectivities of up to 95%. Moreover, selectivity to the head-to-head products (2,5-dimethylhexenes) is remarkably high with up to 99%. Additionally, novel C12 isobutene trimers are also formed with a very high selectivity for the linear linkage of up to 99%. The trimer structure (2,5,8-trimethylnonenes) reflects the stepwise characteristic of the reaction mechanism.

The dimerization of olefins by transition metal complexes is of considerable industrial interest. Olefins such as propene and 1-butene are dimerized on large scale to give mainly branched products for gasoline blending or as feedstocks for alcohol production. While highly branched products are favored in fuels, a higher linearity of products is more desirable as precursors for plasticizers. Although several catalysts are known to generate branched dimers, only a few catalysts are capable of producing linear dimers from 1-alkenes. Keim and co-workers used nickel acetylacetonate complexes for the selective linear oligomerization of 1 alkenes.[2] For instance, 1-butene is dimerized using the one-component catalyst (4-cyclooctene-1-yl)(1,1,1,5,5,5-hexafluoro-2,4-acetylacetonato)nickel **1** with 75-80% linearity.

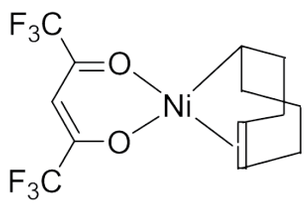

Figure 1: One component nickel catalyst **1**

In this work, catalyst **1** and related systems have been applied to isobutene for the first time. Higher selectivities for the linear dimers in comparison to other 1-alkenes were obtained and carbocation reactivity was successfully suppressed (Figure 2).

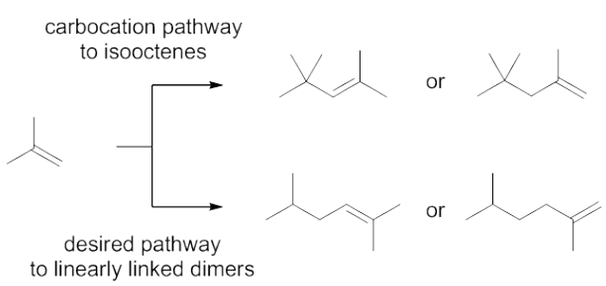

Figure 2: Pathways of isobutene dimerization.

As expected, linearly linked dimers (i.e. 2,5 dimethylhexenes) were the main products with dimer selectivities of up to 95%. Moreover, linearity within the dimer-fraction is remarkably high with up to 99%. Additionally, novel C12-isobutene trimers (2,5,8-trimethylnonenes) are also formed with very high selectivity for the linear linkage of up to 99% (Table1).

Table 1.
Di- and trimerization of isobutene using nickel complex **1**.

No.	T (°C)	X (%)	TOF	S_{dimer} (%)	l:b	$S_{trimers}$ (%)	l:b[b]
1#	120	35	18	94	98:2	6	97:3
2	60	16	27	94	98:2	6	97:3
3	70	70	117	95	99:1	5	97:3
4	75	71	118	93	98:2	7	97:3
5	80	34	57	94	98:2	6	97:3
6	100	20	33	94	98:2	6	97:3
7+	25	38	38	95	99:1	5	97:3

Reaction conditions: 0.3 mol% **1**, *t* = 2 h, 7 g (125 mmol) isobutene, neat. # = 1.0 mol% **1**. + = $Ni(hfacac)_2/Et_2AlOEt$ 1:3, 0,5 mol% Ni.
TOF in [mol isobutene /(mol Ni * h)]. l:b describes the ratio of linear linked products to branched linked products.

Highest turnover frequencies were observed within a narrow temperature range of 70 – 75°C. Neither dimers nor trimers selectivities were affected by temperature, proving deactivation processes being responsible for lower TOFs.

Lower reaction temperatures can be realised by employing a related catalytic system, derived from nickel precursors activated *in situ* by aluminium alkyls. Comparable selectivities and TOFs can be achieved, showing the catalytic nickel-hydride species to be the same in both cases.

Publications:
A. Behr, N. Rentmeister, T. Seidensticker, J. Vosberg, S. Peitz, D. Maschmeyer, Chem. Asian J., 2014, 9, 596-601

Contact:
arno.behr@bci.tu-dortmund.de

This work has been financially supported by Evonik Industries

Thermodynamics (TH)

Salt Influence on Thermodynamics of Biological Solutions

Experiments and Predictions of thermodynamic properties

Christoph Held, Thomas Reschke, Gabriele Sadowski

There is already a deep understanding and a broad availability of thermodynamic properties and phase equilibria of mixtures with chemical components. In contrast, systematic data and quantitative thermodynamic models are still missing for multi-component biological solutions. In this work the salt influence on thermodynamic properties and phase equilibria of aqueous amino acid solutions were measured and predicted by the thermodynamic model ePC-SAFT. Considered aqueous systems contained one amino acid (glycine, L-/DL-alanine, L-/DL-valine, or L-proline) and one of 13 inorganic salts. ePC-SAFT was applied without fitting parameters to the considered aqueous salt+amino acid systems.

Thermodynamic properties of binary water+salt and binary water+amino acid solutions have already been investigated in the literature. One example is shown in Figure 1. Obviously, experimental osmotic coefficients of water+amino acid solutions depend linearly on the molality whereas a non-linear dependence can be observed for water+salt solutions. This behavior is due to the Coulomb interactions in salt solutions and can be modeled quantitatively with ePC-SAFT (lines in Figure 1).

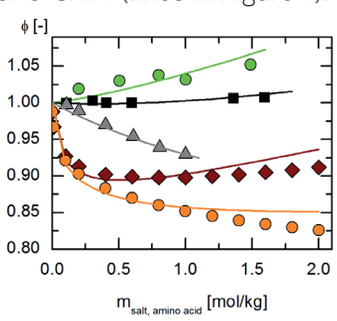

Figure 1: Osmotic coefficients at 25°C and 1 bar of water+salt solutions (orange: $NaNO_3$, dark red: KCl) and water+amino acid solutions (green: proline, black: alanine, grey: glycine). Symbols: data, lines: ePC-SAFT.

In contrast, data and models on multi-component solutions that contain salts *and* amino acids are very scarcely present in the literature. Thus, in this work thermodynamic properties and phase equilibria of biological solutions containing a salt *and* an amino acid were measured. Osmotic coefficients at 25°C were measured by vapor-pressure osmometry.

It can be seen from Figure 2 that the addition of salts (NaCl and $NaNO_3$ in Figure 2) distinctly decreases the experimental osmotic coefficients of valine+water solutions. The salt influence depends on the kind and the concentration of the salt.

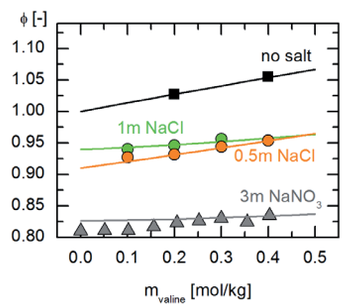

Figure 2: Osmotic coefficients of valine+salt+water solutions at 25°C and constant salt molalities. Symbols: data, lines: ePC-SAFT predictions.

Amino-acid solubilities in water at the presence of salts were measured gravimetrically at 25°C. Figure 3 illustrates that $MgCl_2$ increases the solubility of an amino acid in water.

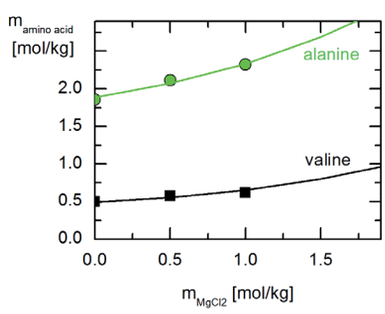

Figure 3: Amino-acid solubility in $MgCl_2$+water solutions at 25°C. Symbols: data, lines: ePC-SAFT predictions.

It becomes obvious from Figures 2 and 3 that ePC-SAFT allows quantitatively predicting the experimental data without fitting parameters to these data.

Contact:
christoph.held@bci.tu-dortmund.de
thomas.reschke@bci.tu-dortmund.de
gabriele.sadowski@bci.tu-dortmund.de

Publications:
Held, C.; Reschke, T.; Müller, R.; Kunz, W.; Sadowski, G.
Measuring and modeling aqueous electrolyte/amino-acid solutions with ePC-SAFT.
J. Chem. Thermodynamics 2014, 68, 1-12

Thermodynamic modelling of protein solubility

Accelerated development of crystallization and precipitation processes for proteins

Marcel Herhut, Christoph Brandenbusch, Gabriele Sadowski

Proteins gained an increased industrial interest especially as therapeutic agents like monoclonal antibodies used against cancer or autoimmune diseases. Within the protein production, the downstream processing can cover up to 80% of the production costs as the purification of proteins is usually achieved by a series of cost-intensive chromatographic steps. A more economical alternative is the precipitation or crystallization of proteins using precipitants, like alcohols, polymers or salts. For these separation steps, protein solubility is the key factor for process development. In this work a new solubility model (solxDLVO) was developed allowing to predict the protein solubility as function of type of precipitant, precipitant concentration, and pH.

The solxDLVO model is a combination of a model to predict the second osmotic virial coefficient B_{22} and a solubility equation to calculate protein solubility based on B_{22}. The use of B_{22} data of the protein is beneficial, as it describes the protein-protein interactions as function of type of precipitant, precipitant concentration and pH value and thus serves as an indicator for the estimation of crystallization/ precipitation conditions.

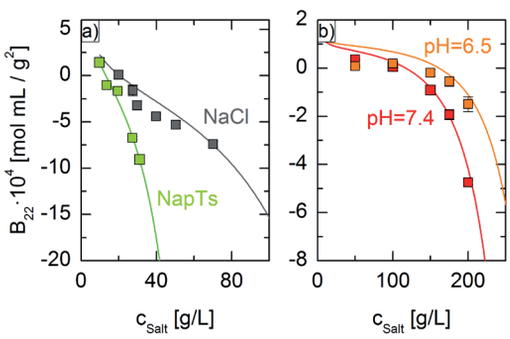

Figure 1: Second osmotic virial coefficient B_{22} of proteins as function of precipitant concentration. a) Lysozyme in aqueous buffer solution with different precipitants. b) Monoclonal antibody in aqueous buffer solution with ammonium sulfate as precipitant at different pH. Symbols: exp.data, solid line: modelling with solxDLVO model.

Compared to conventional screening techniques, the experimental estimation of B_{22} can be easily performed using static light scattering. These measurements are used as input for the solxDLVO model which then allows for a given protein and precipitant the prediction of B_{22} data over the whole range of precipitant concentration and pH value. Figure 1 shows B_{22} values of lysozyme and a monoclonal antibody modelled using the solxDLVO model in comparison with experimental data.

Using the so-obtained B_{22} data, protein solubility can be directly predicted for varying precipitant concentrations and pH values using the solxDLVO model. The results are illustrated in Figure 2 and compared with experimental protein solubilities of lysozyme and monoclonal antibody.

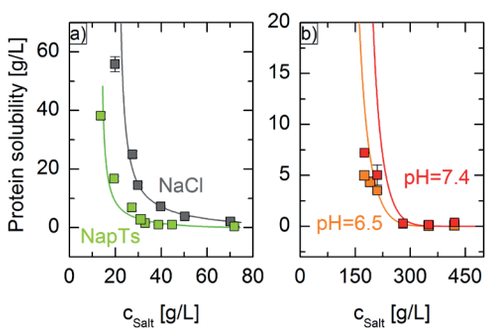

Figure 2: Solubility of proteins as function of precipitant concentration. a) Lysozyme in aqueous buffer solution with different precipitants. b) Monoclonal antibody in aqueous buffer solution with ammonium sulfate as precipitant at different pH. Symbols: exp.data, solid line: modelling with solxDLVO model.

The results show, that the solxDLVO model allows a good estimation of the protein solubility for complex proteins. By using B_{22}, our model can predict the protein solubility for varying precipitant concentrations and pH values. This remarkably reduces the experimental effort for the development of protein crystallization or precipitation processes.

Publications:
Herhut, M.; Brandenbusch, C.; Sadowski, G., Predicting protein solubility and crystallization behavior based on the second osmotic virial coefficient, Oral presentation, International Symposium on the Separation of Proteins, Peptides and Polynucleotides, Boston, MA, USA (2013)

Herhut, M.; Brandenbusch, C.; Sadowski, G., Vorhersage der Löslichkeit und des Kristallisationsverhaltens von Proteinen, Oral presentation, Thermodynamik-Kolloquium, Hamburg, Germany (2013)

Contact:
marcel.herhut@bci.tu-dortmund.de
christoph.brandenbusch@bci.tu-dortmund.de
gabriele.sadowski@bci.tu-dortmund.de

Thermodynamics of pharmaceutical cocrystals

Modeling and predicting the solubility behaviour of pharmaceutical cocrystals

Linda Lange, Gabriele Sadowski

Pharmaceutical cocrystals represent an emerging class of solid drug formulations. They can significantly increase the number of possible crystal forms for a particular active pharmaceutical ingredient (API), each with different physicochemical properties. The conventional methods for a successful cocrystal generation are related to time consuming and expensive experiments. Therefore, within this work the Perturbed-Chain Statistical Associating Fluid Theory (PC-SAFT) is applied to model and to predict the cocrystal solubility for a more efficient cocrystal generation.

Cocrystals consist of the API and at least one coformer (CF) in a defined stoichiometry and they exist only in the solid form. The cocrystal formation is modeled as a chemical reaction of its components, the API and the CF (Eq. 1). The API and CF coefficients, ν_{API} and ν_{CF}, correspond to the API and CF stoichiometry in the cocrystal.

$$\nu_{API}\,API^{Liquid} + \nu_{CF}\,CF^{Liquid} \overset{K_a}{\longleftrightarrow} Cocrystal^{Solid} \qquad \text{Eq. 1}$$

The equilibrium of this reaction is considered by the so-called activity product K_a. This can be calculated using only one cocrystal solubility point, regardless of the solvent (Eq. 2). Knowing K_a, the whole cocrystal solubility line can be modeled.

$$K_a = \prod a_i^{\nu_i} = (x_{API}\gamma_{API})^{\nu_{API}} \cdot (x_{CF}\gamma_{CF})^{\nu_{CF}} \qquad \text{Eq. 2}$$

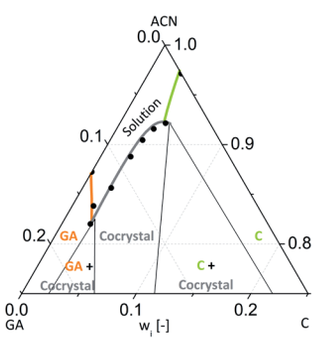

Figure 1: Concentration diagram (weight fractions) of caffeine (C) and glutaric acid (GA) with a 1:1 cocrystal in acetonitrile (ACN) at 298 K. Symbols: exp. data. Lines: modeled solubility lines of C, GA and their cocrystal. All the phases are denoted.

The knowledge of the API/CF/solvent concentration range in which the cocrystal exists in the stable form is the key for cocrystal generation. The stable cocrystal area is determined by the CF, the API and the cocrystal solubility lines, as well as by the cocrystal stoichiometry ν_{CF}:ν_{API}. Figure 1 displays the modeling results for the example system caffeine/glutaric acid (1:1 cocrystal) in acetonitrile at 298 K. The modeling results are in good agreement with the experimental data. The solubility of API in the presence of the coformer and vice versa as well as the cocrystal solubility can be successfully described.

Given the fact that the activity product does not depend on the solvent, the cocrystal solubility can also be predicted in other solvents. The cocrystal solubility for other temperatures can be predicted by using the Gibbs-Helmholtz equation. This enables the K_a calculation at any temperature with a K_a^{ref} at a reference temperature, without further measurements. The activity product K_a for the prediction of the cocrystal solubility at 288 K (Fig. 2) is calculated with the data at the reference temperature of 298 K (Fig. 1).

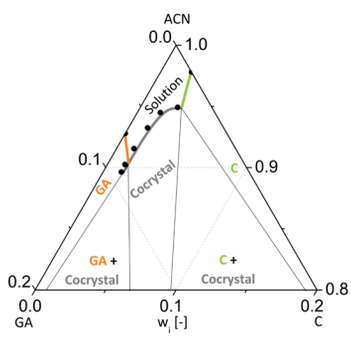

Figure 2: Concentration diagram (weight fractions) of caffeine (C) and glutaric acid (GA) with a 1:1 cocrystal in acetonitrile (ACN) at 288 K. Symbols: exp. data. Lines: modeled solubility lines of C and GA, and the predicted solubility line of the cocrystal. All the phases are denoted.

In summary, all modeled and predicted results are in good agreement with the experimental data. Thus, a reliable determination of the stable cocrystal area is enabled which allows for an efficient cocrystal generation.

Contact:
linda.lange@bci.tu-dortmund.de
gabriele.sadowski@bci.tu-dortmund.de

Publications:
Lange, L.; Sadowski, G.; "Modellierung und Vorhersage des Löslichkeitsverhaltens pharmazeutischer Cokristalle", Jahrestreffen der ProcessNet-Fachgruppe Kristallisation, Münster, Germany (2014).
Lange, L.; Sadowski, G.; "Thermodynamic Modeling for Efficient Cocrystal Generation", 9th PBP World Meeting, Lisbon, Portugal (2014).

Solubility enhancement of amorphous versus crystalline pharmaceuticals

Raphael Paus, Yuanhui Ji, Gabriele Sadowski

Amorphous pharmaceuticals are advantageous compared to their crystalline forms in terms of bioavailability, solubility and dissolution rate. However, so far no reliable thermodynamic modeling was reported that can quantitatively describe and predict the increased solubility of the amorphous form versus the crystalline form. In this project, the aqueous solubilities of crystalline and amorphous pharmaceuticals were for the first time predicted in good accordance with experimental data.

The objective of this work was to predict the *in vitro* performance with regard to the solubility of amorphous pharmaceuticals compared to their crystalline form using a thermodynamic approach. Here, the Perturbed-Chain Statistical-Associating Fluid Theory (PC-SAFT) was used to calculate the solubility of the crystalline active pharmaceutical ingredient (API) and to predict the solubility of its amorphous form.

In contrast to the common approach and in agreement with the thermodynamic phase behavior (as schematically shown in Figure 1), the amorphous API was assumed to form an amorphous liquid-liquid equilibrium with the solvent which is metastable with respect to the solubility line of the crystalline API. The latter was calculated based on the well-known solid-liquid equilibrium relationship.

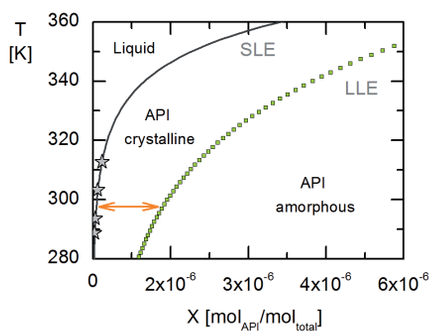

Figure 1: Predicted phase diagram of glibenclamide in water. Stars represent experimental solubility data. The full grey line and the dashed green line are PC-SAFT predictions for the solid-liquid equilibrium (SLE) and liquid-liquid equilibrium (LLE), respectively.

Based on the phase diagram shown in Fig. 1, the solubility ratio between amorphous and crystalline API can easily be determined as shown by the orange arrow from the predicted amorphous and crystalline API solubilities.

Moreover, the activity coefficients of the API which account for the influence of solvent and additives in solution were considered in the calculation of the solubility ratio with PC-SAFT. They are commonly neglected in literature models which usually lead to high deviations between experimental and theoretical results (as shown in Figure 2).

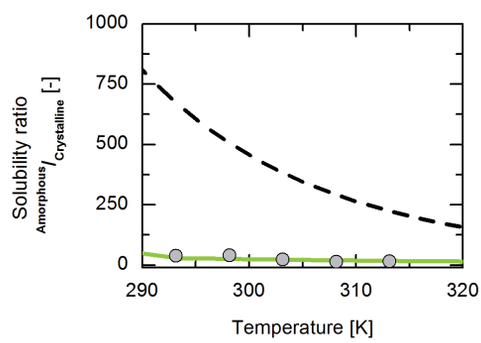

Figure 2: Solubility ratio of amorphous and crystalline glibenclamide in water. Circles represent experimental data. The full green line shows the PC-SAFT prediction. The dashed line represents the modeling results from literature.

The results of this work show that PC-SAFT enables an accurate estimation of the solubility enhancement of amorphous APIs compared to their crystalline form. Here, the solubility of different amorphous pharmaceuticals could be, for the first time, predicted in high accuracy compared to experimental data.

Publications:
Paus, R.; Ji, Y.; Sadowski, G.; Solubility and dissolution of amorphous pharmaceuticals – a novel thermodynamic approach to predict the performance in vitro; AAPS Annual Meeting, Nov. 10-14 2013, San Antonio, USA

Contact:
raphael.paus@bci.tu-dortmund.de
ji.yuanhui@bci.tu-dortmund.de
gabriele.sadowski@bci.tu-dortmund.de

Phase behavior of solid dispersions

Anke Prudic, Yuanhui Ji, Gabriele Sadowski

Most of the promising active pharmaceutical ingredients (APIs) are poorly water soluble and/or have a slow dissolution rate in aqueous media. To circumvent this problem, the API can be formulated into its amorphous form, which is stabilized by polymers. This formulation is usually called a solid dispersion. To prevent recrystallization or phase separation during storage, the knowledge of phase behavior is essential but hard to measure. In this work the phase behavior of solid dispersions was predicted using the thermodynamic model PC-SAFT as function of API, (co)polymer kind as well as relative humidity and verified with experimental data.

The formulation of long-term stable solid dispersions requires the knowledge of the phase behavior. This can help to find an appropriate polymer for an API and also to choose the best storage conditions. The schematic phase behavior of a solid dispersion is shown in Figure 1. Below the solubility line, the amorphous API tends to recrystallize. The liquid-liquid-equilibrium (LLE) line encloses an area where amorphous-amorphous phase separation might occur. Below the glass transition temperature Tg the molecular mobility is reduced so that the amorphous state of the API can be stabilized for a certain time range of weeks or even years.

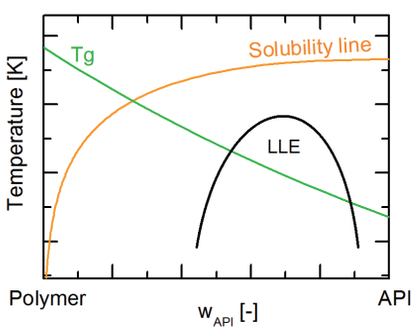

Figure 1: Schematic phase behavior of API/polymer-solid dispersions. Orange line: solubility line of crystalline API in polymer, green line: glass transition temperature of solid dispersion, grey line: LLE region.

In this work the phase behavior of solid dispersions of indomethacin in different polymers was modeled and in the case of copolymer PVPVA 37 (30 wt-% vinyl pyrrolidone and 70 wt-% vinyl acetate monomers) even predicted (Figure 2).

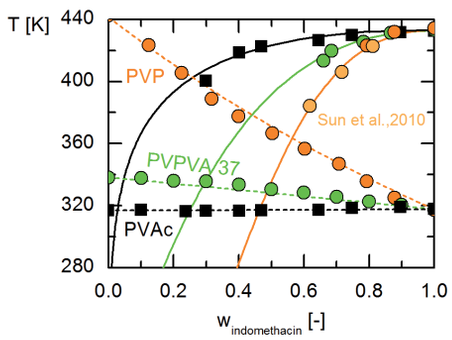

Figure 2: Solubility and Tg modeling of indomethacin in different polymers. Full lines: PC-SAFT calculations of crystalline API solubility, dashed lines: predictions of Tg with Gordon-Taylor-equation, symbols: exp. data

It becomes obvious, that the type of polymer has a significant influence on the API solubility and this can be quantitatively described using PC-SAFT.

Solid dispersions tend to absorb water, which also influences the phase behavior. The amount of absorbed water as function of temperature, polymer type, API concentration and relative humidity can be predicted by PC-SAFT in agreement with the experimental data as shown in Figure 3.

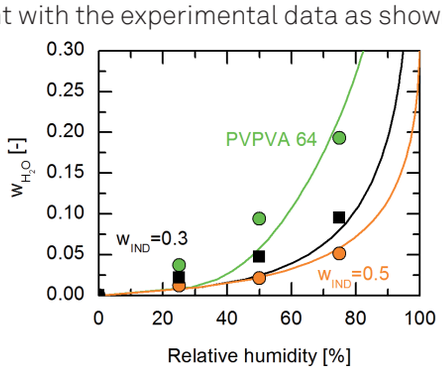

Figure 3: Water sorption of copolymer PVPVA 64 and its solid dispersions with indomethacin as function of relative humidity. Symbols: exp. data, lines: PC-SAFT predictions.

The results of this work show that thermodynamic modeling helps to screen for an appropriate polymer to formulate a solid dispersion and also to choose appropriate storage conditions to ensure a long-term stability of the amorphous state of an API.

Contact:
anke.prudic@bci.tu-dortmund.de
ji.yuanhui@bci.tu-dortmund.de
gabriele.sadowski@bci.tu-dortmund.de

Publications:
Prudic, A.; Ji, Y.; Sadowski, G.; Phase behavior of solid dispersions dependent on relative humidity; AAPS Annual Meeting, Nov. 10-14 2013, San Antonio, USA

Modeling Aqueous Two-Phase Systems

Thomas Reschke, Christoph Brandenbusch, Gabriele Sadowski

The extraction using aqueous two-phase systems is a promising strategy to enable a more cost-effective purification of biomolecules. To facilitate the design of these extraction processes, thermodynamic models can be applied to determine and predict the phase composition of both aqueous phases. The use of predictive models allows for a significant reduction of time-consuming and expensive experiments.

The most common aqueous two-phase systems (ATPS) are formed by water, a salt and a polymer. Polymers which were adapted in ATPS are polyethylene glycol (PEG), polypropylene glycol (PPG), and poly(ethylene glycol-co-propylene glycol) copolymers (EG-PG-Copolymers). For modeling these polymers/copolymers, the different groups within the polymer backbones are explicitly accounted for by considering different polymer segments (see Figure 1). Polymer segments considered are end-group segments (ES), ethylene glycol chain segments (EG-CS) and propylene glycol chain segments (PG-CS).

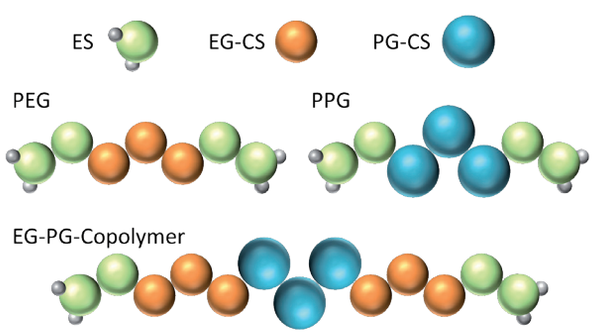

Figure 1: Modelling approach of PEG, PPG, and EG-PG-Copolymers. All polymers are assembled as combination of three different segment types (ES, EG-CS, and PG-CS).

By applying these different segment types, various homopolymers and copolymers can be assembled. This allows for a significant reduction of required modeling parameters as no individual parameters have to be fitted for new polymers composed of these segments.

Figure 2 shows the results of the modeling for an ATPS containing PEG/Na_2SO_4 and PPG/Na_2SO_4. It can be seen that the two-phase compositions obtained with ePC-SAFT are in good agreement with the experimental data.

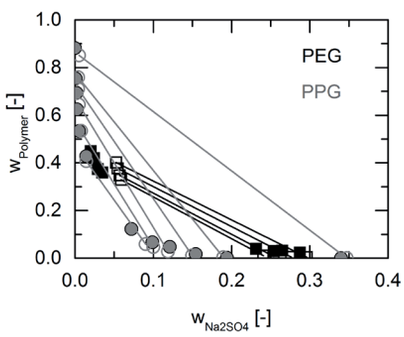

Figure 2: ATPS containing PEG/Na_2SO_4 (squares) and PPG/Na_2SO_4 (circles). The experimental two-phase compositions are given as full symbols; the modeled two-phase compositions are given as open symbols with lines.

Moreover, the application of the modeling approach for the prediction of ATPS containing EG-PG-copolymers (see Figure 3) also results in a very good agreement with experimental data.

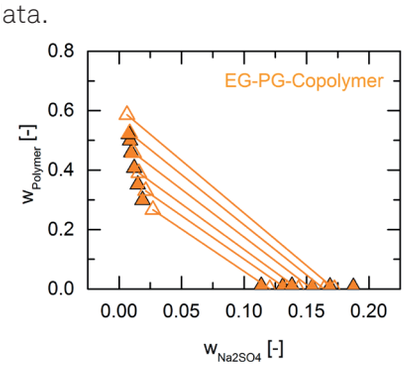

Figure 3: ATPS containing EG-PG-Copolymer/Na_2SO_4. The experimental two-phase compositions are given as full symbols; the modeled two-phase compositions are given as open symbols with lines.

The results of this work can now be used for predictive modeling of ATPS. This will allow for faster and economic development of extraction processes based on ATPS by drastically reducing the experimental effort.

Publications:
Reschke, T.; Brandenbusch, C.; Sadowski, G. Modeling Aqueous Two-Phase Systems: I PEG and inorganic salts as ATPS former. Fluid Phase Equilib. (2014), http://dx.doi.org/10.1016/j.fluid.2014.02.016

Reschke, T.; Brandenbusch, C.; Sadowski, G. Modeling Aqueous Two-Phase Systems: II Polyether and inorganic salts as ATPS former. Fluid Phase Equilib. Submitted 2014

Contact:
thomas.reschke@bci.tu-dortmund.de
christoph.brandenbusch@bci.tu-dortmund.de
gabriele.sadowski@bci.tu-dortmund.de

Impressum

Fakultät für Bio- und Chemieingenieurwesen
TU Dortmund

www.bci.tu-dortmund.de

Redaktion: Prof. Jörg C. Tiller